GNGA FOR SEMILINEAR ELLIPTIC PDE ON A FRACTAL REGION: SYMMETRY AND AUTOMATED BRANCH FOLLOWING.

JOHN M. NEUBERGER, NÁNDOR SIEBEN, AND JAMES W. SWIFT

ABSTRACT. We apply the GNGA (Gradient-Newton-Galerkin-Algorithm) of Neuberger-Swift to find solutions to a semilinear elliptic Dirichlet problem on the region whose boundry is the Koch snowflake. In a recent paper, we described an accurate and efficient method for generating a basis of eigenfunctions of the Laplacian. In that work, we used the symmetry of the snowflake region to analyze and post-process the basis, rendering it suitable for input to the GNGA. The GNGA uses Newton's method on the eigenfunction expansion coefficients to find solutions to the semilinear problem. This article introduces the bifurcation digraph, an extension of the lattice of isotropy subgroups, which describes the possible symmetries of solutions and the generic symmetry-breaking bifurcations. We use continuation methods to solve the problem of choosing an initial guess for Newton's method, and to find at least one solution of each of the 23 symmetry types that we predict should exist. Such computationally intensive investigations necessitated the writing of automated branch following code, whereby symmetry information was used to reduce the number of computations per GNGA execution and to make intelligent branch following decisions at bifurcation points.

1. INTRODUCTION.

We seek numerical solutions to the semilinear elliptic boundary value problem

$$\Delta u + f(u) = 0 \text{ in } \Omega$$

pde (1.1) $$u = 0 \text{ on } \partial\Omega,$$

where Δ is the Laplacian operator and $\Omega \subset \mathbb{R}^2$ is the (open) region whose boundary $\partial\Omega$ is the Koch snowflake. As far as we know, this article is the first to consider a nonlinear PDE on a region with fractal boundary. In this paper, we will choose the nonlinear function $f : \mathbb{R} \to \mathbb{R}$ to be defined by

nonlinearity (1.2) $$f(u) = \lambda u + u^3,$$

treating the parameter $\lambda = f'(0)$ as a bifurcation parameter. Except for certain aspects of our symmetry analysis, all of our experiments could easily be done for other choices of nonlinearity, in particular, for f non-odd. For convenience, we refer to Ω as the *Koch snowflake region*. It is well known that the eigenvalues of the Laplacian under this boundary condition satisfy

evals (1.3) $$0 < \lambda_1 < \lambda_2 \leq \lambda_3 \leq \cdots \to \infty,$$

and that the corresponding eigenfunctions

efns (1.4) $$\{\psi_j\}_{j\in\mathbb{N}}$$

2000 *Mathematics Subject Classification.* 20C35, 35P10, 65N25.
Key words and phrases. Snowflake, Symmetry, Semilinear Elliptic PDE, GNGA.
Partially supported by NSF Grant DMS-0074326.
May 17, 2005.

are an orthogonal basis of both the Sobolev space $H = H_0^{1,2}(\Omega)$ and the larger Hilbert space $L_2 = L_2(\Omega)$, with the inner products

$$\langle u, v\rangle_H = \int_\Omega \nabla u \cdot \nabla v \, dx \quad \text{and} \quad \langle u, v\rangle_2 = \int_\Omega u \, v \, dx,$$

respectively. Using the Gradient-Newton-Galerkin-Algorithm (GNGA, see [NS]) we seek approximate solutions $u = \sum_{j=1}^{M} a_j \psi_j$ to (1.1) by applying Newton's method to the eigenfunction expansion coefficients of the gradient $\nabla J(u)$ of a nonlinear functional J whose critical points are the desired solutions. The definition of J, the required variational equations, a description of the GNGA, and a brief history of the problem are the subject of Section 2.

The GNGA requires as input a basis spanning a sufficiently large but finite dimensional subspace $\text{span}\{\psi_1, \ldots, \psi_M\}$, corresponding to the first M eigenvalues $\{\lambda_j\}_{j=1}^{M}$. As described in [20], a grid G_N of N carefully placed points is used to approximate the eigenfunctions. These are the same grid points used for the numerical integrations required by Newton's method. Section 3 briefly describes the process we use for generating the eigenfunctions.

Section 4 concerns the effects that the hexagonal symmetry of the snowflake region have on the solutions to equation (1.1) and their bifurcations. The symmetry theory for linear operators found in [20] is summarized and then the extensions required for nonlinear operators are described. In particular, there are 23 different symmetry types of solutions to (1.1). These are traditionally organized in the lattice of isotropy subgroups (see [7]). While this theory is well-known, we give a new way to organize the results in a *bifurcation digraph*. This directed graph generalizes the lattice of isotropy subgroups, in that it includes information about the generic bifurcations among symmetry types.

We use repeated executions of the GNGA or a slightly modified algorithm (parameter-modified GNGA) to follow bifurcation branches containing solutions to (1.1) of any desired symmetry. The solution of the previous execution becomes the initial guess for the next. Typically, we vary λ slightly between executions. Near bifurcation points, we treat λ as a variable and instead fix one of the eigenfunction expansion coefficients. We use our symmetry knowledge to make our computations of gradients and Hessians more efficient, as well as to make intelligent branch following decisions. Starting with the trivial solution, the bifurcating branches are followed automatically, thus eliminating the need to guess approximate solutions for input into Newton's method. In this way solutions with all 23 symmetry types are found automatically. Section 6 describes the automated continuation techniques that makes this possible.

In our experiments, many bifurcation diagrams were generated by applying the techniques mentioned above. A selection of these diagrams are provided in Section 7, along with contour plots of solutions to (1.1) corresponding to each of the 23 symmetry types predicted to exist. We include evidence of the convergence of our algorithm as the number of modes M and grid points N increase.

Many extensions to our work are possible, including enforcing different boundary conditions on the same region, solving similar semilinear equations on other fractal regions, applying the methodology to partial difference equations (PdE) on graphs, and porting the scalar code to a parallel environment. We briefly discuss these and other ideas in the concluding Section 9.

2. GNGA.

GNGA_section

We now present the variational machinery for studying (1.1) and follow with a brief description of the general GNGA. Section 6 contains the details of the implementation of the algorithm for our

specific problem. Let $F(u) = \int_0^u f(s)\,ds$ for all $u \in \mathbb{R}$ define the primitive of f. We then define the action functional $J : H \to \mathbb{R}$ by

Jdef
$$J(u) = \int_\Omega \left\{ \frac{1}{2}|\nabla u|^2 - F(u) \right\} dx. \tag{2.1}$$

The class of nonlinearities f found (for example) in [2, 3, 18] imply that J is well defined and of class C^2 on H. The choice (1.2) we make in this paper belongs to that class. It is well known that critical points of J are in fact solutions to (1.1) (see for example [21]), and vice versa. Take λ_j and ψ_j as in (1.3) and (1.4), with the eigenfunctions normalized in L_2; given a coefficient vector $a \in \mathbb{R}^M$, we expand $u = \sum_{j=1}^M a_j \psi_j$. Integrating by parts, we can see that

JprimeDef
$$J'(u)(\psi_j) = \int_\Omega \{\nabla u \cdot \nabla \psi_j - f(u)\,\psi_j\} = a_j \lambda_j - \int_\Omega f(u)\,\psi_j \tag{2.2}$$

and

JprimePrimeDef
$$J''(u)(\psi_j, \psi_k) = \int_\Omega \{\nabla \psi_j \cdot \nabla \psi_k - f'(u)\,\psi_j\,\psi_k\} = \lambda_j \delta_{jk} - \int_\Omega f(u)\,\psi_j\,\psi_k, \tag{2.3}$$

where δ_{jk} is the Kronecker delta function. Note that there is no need for numerical differentiation when forming gradient and Hessian coefficient vectors and matrices in implementing Algorithm 2.1; this information is encoded in the eigenfunctions.

The heart of our code is Newton's method in the space of eigenfunction coefficients:

algorithm
Algorithm 2.1. (GNGA)

(1) Choose initial coefficients $a = \{a_k\}_{k=1}^M$, and set $u = \sum a_k \psi_k$.
(2) Loop
  (a) Calculate the gradient vector $g = \{J'(u)(\psi_k)\}_{k=1}^M$ from equation (2.2).
  (b) Calculate the Hessian matrix $h = \{J''(u)(\psi_j, \psi_k)\}_{j,\,k=1}^M$ from equation (2.3).
  (c) Exit loop if $||g||$ is sufficiently small.
  (d) Solve $h\chi = g$ for the Newton search direction $\chi \in \mathbb{R}^M$.
  (e) Replace $a \leftarrow a - \chi$ and update $u = \sum a_k \psi_k$.
(3) Calculate $\mathrm{sig}(h)$ and J for the approximate solution.

If Newton's method converges then we expect that u approximates a solution to the PDE (1.1), provided M is sufficiently large and the eigenfunctions and numerical integrations are sufficiently accurate. Our estimate for the Morse index (MI) of the critical point of J is the signature of h, denoted $\mathrm{sig}(h)$, which is defined as the number of negative eigenvalues of h. This measures the number of linearly independent directions away from u in which J decreases (quadratically).

The basic Algorithm 2.1 is modified to take advantage of the symmetry of our problem. The number of integrations required in step (a) and (b) of the loop can be reduced from $M + M^2$ to a smaller number if the initial guess has nontrivial symmetry.

We often use a "parameter-modified" version of the GNGA (pmGNGA). In this modification, λ is treated like an unknown variable and one of the M coefficients a_k is fixed. This allows us to force symmetry-breaking membership on a new branch. Along a given branch, symmetry generally forces many coefficients to be zero. When a bifurcation point is located by observing a change in MI, we can predict the symmetry of the bifurcating branches using the symmetry of the critical eigenfunctions. By forcing a small nonzero component in the larger invariant subspace (orthogonal to the old branch's smaller invariant subspace), we can assure that the pmGNGA will not converge

to a solution lying on the old branch. Another benefit of the pmGNGA is that it can handle a curve bifurcating to the right as well as one bifurcating to the left. Finally, the branches that bifurcate to the right often have saddle node bifurcations where they turn around and go to the left. The pmGNGA can follow such branches while the normal GNGA cannot.

The implementation of pmGNGA is not difficult. The M equations are still

$$g_i = J'(u)(\psi_i) = 0,$$

but the M unknowns are

$$\tilde{a} = (a_1, \ldots, a_{k-1}, \lambda, a_{k+1}, \ldots, a_M),$$

and the value of one coefficient, a_k, is fixed. Consequently, we replace the Hessian matrix h with a new matrix $\tilde{h}$ where the k-th column is set to $\partial g_i/\partial\lambda = -a_i$:

$$\tilde{h}_{ij} = \begin{cases} h_{ij} & \text{if } j \neq k \\ -a_i & \text{if } j = k \end{cases}.$$

The search direction $\tilde{\chi}$ is the solution to the system $\tilde{h}\tilde{\chi} = g$. The pmGNGA step is

$$\tilde{a} \leftarrow \tilde{a} - \tilde{\chi},$$

and then u and λ are updated. After Newton's method converges, the k-th column of the original h_{ij} is calculated and the MI of the solution, $\mathrm{sig}(h)$, is computed.

We conclude this section with a very brief history of the analytical and numerical aspects of the research into (1.1) given our type of nonlinearity f. Our introduction to this general subject was [2], where a sign-changing existence result was proven. This theorem is extended in [3]; we indicate briefly in Section 7 where this so-called CCN solution can be found on our bifurcation diagrams. The GNGA was developed and announced in [19], wherein a much more detailed description of the variational structure and numerical implementation can be found. The computational efforts related to this current project are somewhat more sophisticated. The more important aspects of our improvements are explained in Sections 4 and 6. This article might be the first of our published works concerning GNGA for general regions; a successful but as yet unsubmitted investigation for the case Ω is a disk in $\mathbb{R}^2$ and the work in progress [12] where Ω is a Bunimovich stadium further demonstrate this generality. The article [4] was our first success in using symmetry to find higher MI solutions. The details concerning the grid, basis generation, and subsequent symmetry analysis for the snowflake are in [20]. The article [11] provides a historical overview of the authors' experimental results using variants of the Mountain Pass Algorithm (MPA, MMPA, HLA) and the GNGA, as well as recent analytical results and a list of open problems; the references found therein are extensive.

3. The Basis of Eigenfunctions.

basis_section

In [20], we describe theoretical and computational results that lead to the generation of a basis of eigenfunctions solving

lpde

$$\Delta u + \lambda u = 0 \text{ in } \Omega, \quad u = 0 \text{ on } \partial\Omega. \tag{3.1}$$

The paper details the grid technique and symmetry analysis that accompanied the effort; we briefly summarize those results in this section.

The Koch snowflake is a well known fractal, with Hausdorff dimension $\log_3 4$. Following Lapidus, Neuberger, Renka, and Griffith [9], we take our snowflake to be inscribed in a circle of radius $\frac{\sqrt{3}}{3}$

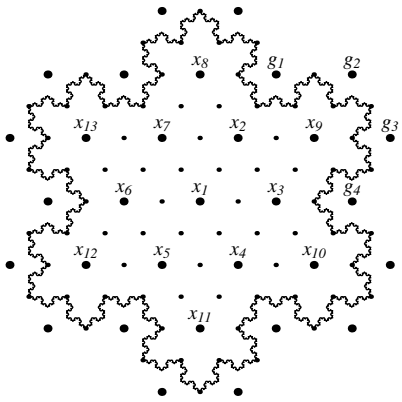

FIGURE 1. The Koch snowflake $\partial\Omega$ with $N = 13$ labelled grid points $\{x_i\}_{i=1}^{13}$ at level $\ell = 2$. At this level, the grid used by [9] consists of the $N_{\mathrm{LNR}}(2) = 37$ large and small points inside the snowflake, along with the 48 small points on $\partial\Omega$. The points outside of the snowflake, some labelled g_i, are ghost points we use to enforce the boundary conditions; these ghost points are not used by our nonlinear code. grid

ℓ	1	2	3	4	5	6
N	1	13	133	1261	11605	105469

TABLE 1. The number of interior grid points with spacing $h = h_{\mathrm{NSS}}(\ell) = 2/3^\ell$. We typically use level $\ell = 5$ in our nonlinear experiments. grid_table

centered about the origin. With this choice, the polygonal approximations used in the fractal construction have side length that are powers of 1/3. We use a triangular grid G_N of N points to approximate the snowflake region. Then, we identify $u : G_N \to \mathbb{R}$ with $u \in \mathbb{R}^N$, that is,

$$u(x_i) = u_i \tag{3.2}$$ ui

at grid points $x_i \in G_N$. Figure 1 depicts a low level grid used in [20] to compute eigenfunctions; we use this same grid for our nonlinear experiments. The number of grid points on other levels are in Table 1.

Our method of imposing the zero-Dirichlet boundary conditions can be summarized as

$$-\Delta u(x) \approx \frac{2}{3h^2}((12 - \text{number of interior neighbors})u(x) - \sum\{\text{interior neighbor values of } u\}). \tag{3.3}$$ template

Using the differencing scheme in (3.3) and the grid depicted in Figure 1, we computed [20] eigenvalues and eigenfunctions for (3.1) using ARPACK. Table 2 lists approximations of the first ten eigenvalues; these values are primary bifurcation points. The ARPACK is based upon an algorithmic variant of the Arnoldi process called the Implicitly Restarted Arnoldi Method (see [14]) and is ideally suited for finding the eigen-pairs of the large sparse matrices associated with the discretization of the Laplacian.

k	1	2	3	4	5	6	7	8	9	10
λ_k^{R}	39.4	97.4	97.4	165.4	165.4	190.4	208.6	272.4	272.4	312.4

TABLE 2. Approximate values for the first ten eigenvalues to the Dirichlet problem. Richard_D1 For more values with greater precision see [20].

4. Symmetry: The Lattice of Isotropy Subgroups and The Bifurcation Digraph.

symmetry_section This section describes equivariant bifurcation theory (see, for example [7] or [8]) as it applies to the branching of solutions to equation (1.1). We are able to describe in general all expected symmetry types of solutions to 1.1, as traditionally arranged in a lattice of isotropy subgroups. In the first subsection we introduce the *bifurcation digraph*, essentially a refinement of the lattice, which shows every possible generic bifurcation from one symmetry type to another as a directed edge which is labelled with information about the bifurcation. This digraph is of interest in its own right and summarizes the essential information required by our automated branch following code. In this project, GAP (Groups, Algorithms, and Programming, see [6]) is used to verify our symmetry analysis; in our continuing projects GAP is a necessary tool when the symmetry calculations are too complicated to be done by hand. In the second subsection, we apply this methodology to the snowflake domain being considered in this paper. The analysis shows that solutions fall into 23 symmetry types, and that there are 64 generic symmetry breaking bifurcations.

4.1. Group Actions and the Bifurcation Digraph.

Let Γ be a finite group and V be a vector space. A *representation* of Γ is a homomorphism $\alpha : \Gamma \to GL(V)$. Every representation α corresponds to a unique *group action* of Γ on V by the rule $\gamma \cdot v := \alpha(\gamma)(v)$ for all $\gamma \in \Gamma$ and $v \in V$. We will usually use the action rather than the representation. The *group orbit* of v is $\Gamma \cdot v = \{\gamma \cdot v \mid \gamma \in \Gamma\}$.

Let us recall some facts about group actions, following [7]. Let Γ be a finite group acting on a vector space V. The *isotropy subgroup* or *stabilizer* of $v \in V$ is

$$\mathrm{Stab}(\Gamma, v) = \{\gamma \in \Gamma \mid \gamma \cdot v = v\}.$$

Other notations for what we call $\mathrm{Stab}(\Gamma, v)$ are Γ_v or the "little group" of v. The Γ is necessary when several groups act on the same space. If the group is understood, we may simply write $\mathrm{Stab}(v)$ in place of $\mathrm{Stab}(\Gamma, v)$. The isotropy subgroup measures how much symmetry v has. The *stabilizer of a subset* $W \subseteq V$ is then defined as $\mathrm{Stab}(\Gamma, W) = \{\gamma \in \Gamma \mid \gamma \cdot W = W\}$. This must be distinguished from the *point stabilizer of a subset* $\mathrm{pStab}(\Gamma, W) = \bigcap\{\mathrm{Stab}(\Gamma, v) \mid v \in W\}$. Another commonly used notation is Γ_W for the stabilizer and $\Gamma_{(W)}$ for the point stabilizer. Note that $\mathrm{pStab}(\Gamma, W)$ is always normal in $\mathrm{Stab}(\Gamma, W)$, and $\mathrm{Stab}(\Gamma, W)/\mathrm{pStab}(\Gamma, W)$ acts faithfully on W.

If Σ is a subgroup of Γ then the *fixed point subspace of* Σ *in* V is

$$\mathrm{Fix}(\Sigma, V) = \{v \in V \mid \ \gamma \cdot v = v \text{ for all } \gamma \in \Sigma\}.$$

Often, we will drop the V when the space on which Γ acts is clear.

An *isotropy subgroup* of the Γ action on V is a stabilizer of some point $v \in V$. For some group actions, not every subgroup of Γ is an isotropy subgroup. A necessary and sufficient condition for Σ to be an isotropy subgroup of a Γ action on V is that $\Sigma = \mathrm{pStab}(\Gamma, \mathrm{Fix}(V, \Sigma))$, or when Γ and

V are understood, simply

isosub (4.1) $$\Sigma \text{ is an isotropy subgroup} \iff \Sigma = \mathrm{pStab}(\mathrm{Fix}(\Sigma)).$$

An operator $T : V \to V$ is Γ-*equivariant* if $T(\gamma \cdot v) = \gamma \cdot T(v)$ for all $\gamma \in \Gamma$. The isotropy subgroups and fixed point subspaces are important because of the following simple yet powerful results. See [7] or [8].

fps **Proposition 4.2.** *Suppose* Γ *acts linearly on* V, $T : V \to V$ *is* Γ*-equivariant and* Σ *is an isotropy subgroup of* Γ. *Then*

(a) *If* $v \in \mathrm{Fix}(\Sigma)$ *then* $T(v) \in \mathrm{Fix}(\Sigma)$.
(b) $\mathrm{Stab}(\mathrm{Fix}(\Sigma)) = N_\Gamma(\Sigma)$, *the normalizer of* Σ *in* Γ.
(c) $T|_{\mathrm{Fix}(\Sigma)}$ *is* $N_\Gamma(\Sigma)$*-equivariant.*
(d) $T|_{\mathrm{Fix}(\Sigma)}$ *is* $N_\Gamma(\Sigma)/\Sigma$*-equivariant, and* $N_\Gamma(\Sigma)/\Sigma$ *acts faithfully on* $\mathrm{Fix}(\Sigma)$.

Two subgroups Σ_1, Σ_2 of Γ are conjugate ($\Sigma_1 \sim \Sigma_2$) if $\Sigma_1 = \gamma\Sigma_2\gamma^{-1}$ for some $\gamma \in \Gamma$. Note that $\mathrm{Stab}(\gamma \cdot v) = \gamma\,\mathrm{Stab}(v)\gamma^{-1}$. We define the *symmetry type* of $v \in V$ to be the conjugacy class of $\mathrm{Stab}(v)$. Thus, every element of a group orbit $\Gamma \cdot v$ has the same symmetry type.

Let $\mathcal{S} = \{S_i\}$ denote the set of all symmetry types. The set $\mathcal{S}$ is a partially ordered set, with $S_i \le S_j$ if there exits $\Sigma \in S_i$ and $\Gamma \in S_j$ such that $\Sigma \le \Gamma$. The inclusion lattice of $\mathcal{S}$ is called the *lattice of isotropy subgroups* [7].

Consider a bifurcation problem of the form $g(\lambda, u) = 0$, where $g(\lambda, \cdot) : V \to V$ is a Γ-equivariant operator and λ is a real bifurcation parameter. Definitely, we have in mind the PDE defined by (1.1) and (1.2), with $\Gamma = \mathbb{D}_6 \times \mathbb{Z}_2$, V is the appropriate function space, and g is the gradient vector defined in Section (2). The specific calculations for this case are the material of the next subsection. We define a *branch of solutions* to be a path of points $(\lambda, u) \in \mathbb{R} \times H$ where the functions u are solutions with a given symmetry. A branch of solutions B_1 has a *symmetry-breaking bifurcation* at the *bifurcation point* $(\lambda^*, u^*) \in B_1$ if a different branch of solutions, B_2, has (λ^*, u^*) as a limit point but $(\lambda^*, u^*) \notin B_2$. We say that branch B_2 is *created* at this bifurcation.

The trivial solution to (1.1) is $u \equiv 0$, and the *trivial branch* is $\{\{\lambda, 0) \mid \lambda \in \mathbb{R}\}$. A *primary branch* is a branch that is created at a symmetry-breaking bifurcation of the trivial branch.

At a bifurcation point, $D^2J(\lambda^*, u^*) = Dg(\lambda^*, u^*)$ is not invertible. If Dg is invertible then the implicit function theorem guarantees the existence of a unique local solution branch. We define the null space of $Dg(\lambda^*, u^*)$ as the *critical eigenspace*, which we denote by E. The zero eigenvalues and corresponding eigenfunctions in E are termed *critical*. We define the *symmetry group of the bifurcation* as $\mathrm{Stab}(u^*)/\mathrm{Stab}(E)$. That is, the group elements that fix E pointwise act as the identity in the symmetry group of the bifurcation. At a symmetry-breaking bifurcation we can translate (λ^*, u^*) to the origin, and do an equivariant Liapunov-Schmidt reduction to obtain reduced bifurcation equations $\tilde{g} : \mathbb{R} \times E \to E$ where $D\tilde{g}(0, 0) = 0$, and $\tilde{g}$ is $\mathrm{Stab}(u^*)/\mathrm{Stab}(E)$-equivariant. The symmetry of the bifurcation, $\mathrm{Stab}(u^*)/\mathrm{Stab}(E)$, can be computed by purely group-theoretic calculations without actually computing the Liapunov-Schmidt reduction.

Definition 4.3. PUT EBL stuff here, then define bifurcation digraph.

We use GAP to analyze all of the irreducible representations of Γ_i for one isotropy subgroup in each of the symmetry types S_i. This yields a wealth of information that is summarized in the bifurcation digraph. In the next section, we develop the bifurcation digraph for the snowflake domain problem where $\Gamma = \mathbb{D}_6 \times \mathbb{Z}_2$ (see Fig. 2). Each edge is labelled with the symmetry group

of the bifurcation. This is important because the symmetry constrains the type of branching that can occur, and the normal form equations of bifurcations with many small symmetry groups have been analyzed.

Typically, a change of MI is an indicator for the presence of a symmetry breaking bifurcation. The MI also changes on a branch at a saddle-node "bifurcation." The branch of solutions is not monotonic in λ at a saddle-node bifurcation, but there is no intersection of branches and hence no symmetry-breaking bifurcation. Our code can follow the branch as it turns over at a saddle-node bifurcation using the pmGNGA.

A characteristic of a saddle-node bifurcation is that the critical eigenvector lies in $\mathrm{Fix}(u^*)$. Hence $\Gamma' = \Gamma$, and a saddle-node bifurcation is a bifurcation with trivial symmetry. **I think Γ' is never defined.** In contrast, at a symmetry-breaking bifurcation, the critical subspace E is orthogonal the $\mathrm{Fix}(u^*)$, and Γ/Γ' is nontrivial.

When a solution with symmetry Γ has a symmetry-breaking bifurcation, it is important to analyze the action of Γ on the critical eigenspace E. The lattice of isotopy subgroups of this action are computed. If $\mathrm{Fix}_E(\Sigma)$ is a one-dimensional fixed point subspace, then the Equivariant Branching Lemma (EBL) says that "generically" a solution with isotropy Σ will be created at the bifurcation. We refer the reader to [7] or [8] for a discussion of the EBL and genericity. Suffice it to say that we only expect to see generic properties in our numerical investigations. We define a *maximal isotropy subgroup* of a Γ action to be a maximal *proper* isotropy subgroup. Suppose Γ acts on E with $\mathrm{Fix}_?(\Gamma) = 0$. Then $\dim \mathrm{Fix}_E(\Sigma) = 1$ implies that Σ is a maximal isotropy subgroup of Γ. The converse is not true. For the group $\mathbb{Z}_3$ acting on $\mathbb{R}^2$ as rotations , the trivial group $\langle 1 \rangle$ is a maximal isotropy subgroup of $\mathbb{Z}_3$, but $\mathrm{Fix}(\langle 1 \rangle) = \mathbb{R}^2$. This example is relevant to our PDE (1.1) when a solution with isotropy $\mathbb{Z}_3$ has a symmetry-breaking bifurcation. Typically, such a solution would have a Hopf-bifurcation, but this is not possible in a gradient system, such as our PDE (1.1) wich can be written as $\nabla J(\lambda, u) = 0$. In a symmetry-breaking bifurcation of a gradient system, generically a branch is created with isotropy Σ for every maximal isotropy subgroup of Γ ([7],[10], [24]). We call such solution branches, that are not guaranteed to exist by the equivariant branching lemma, *non-EBL* branches.

In our bifurcation digraph, for every isotropy subgroup $\Gamma \leq \mathbb{D}_6 \times \mathbb{Z}_2$, we compute the isotypic decomposition of U under the action of Γ. The irreducible spaces of the Γ action on U corresponding to the nontrivial irreducible representations of Γ are the possible critical eigenspaces $E_i(\Gamma)$ (where i labels the irreducible representation). We compute the lattice of isotropy subgroups of Γ acting on $E_i(\Gamma)$. The bifurcation digraph has an edge from Γ to every maximal isotropy subgroup Σ of the action on each $E_i(\Gamma)$. The edge is labelled with the symmetry group of the bifurcation, $\Gamma/\mathrm{Stab}(E_i(\Gamma))$. Furthermore, there is an arrow type, either solid, dashed or dotted. The arrow type depends on the quotient group $N_\Gamma(\Sigma)$, which is the effective symmetry group of the PDE, restricted to $\mathrm{Fix}(\Sigma)$, in the neighborhood of a point u with isotropy Γ. The arrow in the bifurcation digraph is solid if $\mathrm{Fix}_{E_i(\Gamma)}(\Sigma)$ is one-dimensional and $N_\Gamma(\Sigma) = \mathbb{Z}_2$. This means that there is a pitchfork bifurcation. There are two bifurcating branches that belong to one group orbit of branches. The arrow in the bifurcation digraph is dashed if $\mathrm{Fix}_{E_i(\Gamma)}(\Sigma)$ and $N_\Gamma(\Sigma) = \langle 1 \rangle$, the trivial group. In this case there are two non-conjugate solution branches. Usually the bifurcation is transcritical, meaning that one branch bifurcates to the left while the other bifurcates to the right. Note that $N_\Gamma(\Sigma)$ must be either $\mathbb{Z}_2$ or the trivial group if the dimension of $\mathrm{Fix}_{E_i(\Gamma)}(\Sigma)$ is one. Finally, the arrow in the bifurcation digraph is dotted if the dimension of $\mathrm{Fix}_{E_i(\Gamma)}(\Sigma)$ is larger than one. This means that we expect a non-EBL solution branch in a gradient system.

4.2. **The Digraph for $\mathbb{D}_6 \times \mathbb{Z}_2$.** The symmetry group of the snowflake region Ω, as well as the set of grid points G_N, is isomorphic to the dihedral group

$$\mathrm{Aut}(\Omega) \cong \mathbb{D}_6 := \langle \rho, \sigma \mid \rho^6 = \sigma^2 = 1, \rho\sigma = \sigma\rho^5 \rangle.$$

It is convenient to define $\tau = \rho^3\sigma$. Note that $\sigma\tau = \tau\sigma = \rho^3$, and ρ^3 commutes with every element in $\mathbb{D}_6$. The standard action of $\mathbb{D}_6$ on the plane is

actionOnPlane

$$\begin{aligned} \rho \cdot (x, y) &= \left(\tfrac{1}{2}x + \tfrac{\sqrt{3}}{2}y, -\tfrac{\sqrt{3}}{2}x + \tfrac{1}{2}y\right) \\ \sigma \cdot (x, y) &= (-x, y) \\ \tau \cdot (x, y) &= (x, -y). \end{aligned} \tag{4.4}$$

In this action ρ is a rotation by $60°$, σ is a reflection across the y-axis, and τ is a reflection across the x-axis.

For a given grid $G_N = \{x_i\}_{i=1}^N$, the $\mathbb{D}_6$ action on the plane (4.4) induces a group action on the set $\{1, \ldots, N\}$ defined by $x_{\nu \cdot i} = \nu \cdot x_i$. There is also a natural action of $\mathbb{D}_6$ on the relevant spaces $U = L_2(\Omega)$ and $U = \mathbb{R}^N$ corresponding to a grid G_N defined by $(\nu \cdot u)(x) = u(\nu^{-1} \cdot x)$ and $(\nu \cdot u)_i = u_{\nu^{-1} \cdot i}$ respectively.

To discuss the effects of symmetry on the nonlinear PDE (1.1) we define the $\mathbb{D}_6 \times \mathbb{Z}_2$ action on $L_2(\Omega)$ and U, where $\mathbb{Z}_2 = \{-1, 1\}$. For all $(\nu, z) \in \mathbb{D}_6 \times \mathbb{Z}_2$, define

$$(\nu, z) \cdot u = z(\nu \cdot u).$$

We will denote $(\nu, 1)$ by ν and $(\nu, -1)$ by $-\nu$. With this natural notation $(-\nu) \cdot u = -(\nu \cdot u)$, which we call simply $-\nu \cdot u$.

Every subgroup of the $\mathbb{D}_6$ action on the function space $L_2(\Omega)$ is an isotropy subgroup. To see this, start with a function u_0 with compact support, such that the support of $\gamma \cdot u_0$ is disjoint for the twelve elements $\gamma \in \mathbb{D}_6$. Then, for any subgroup $\Sigma \leq \mathbb{D}_6$, the function $\sum_{\gamma \in \Gamma} \gamma \cdot u_0$ has isotropy Σ. Note that this argument carries over to the $\mathbb{D}_6$ action on the space of functions on a single group orbit of size 12, which function space can be identified with $\mathbb{R}^{12}$. The same holds for functions on the grid G_N, provided there is at least one group orbit of grid points of size 12. This happens in our grids at level $\ell \geq 3$, which have $N \geq 133$ grid points. In contrast, the $\mathbb{D}_6$ action on $\mathbb{R}^{13}$ corresponding to the level 2 grid shown in Figure 1 does not have $\langle \rho$ as an isotropy subgroup. This is related to the fact that every grid point in Figure 1 is on a line of reflection symmetry.

In what follows, we will use U to stand for a vector space for which every subgroup of $\mathbb{D}_6$ is an isotropy subgroup of the $\mathbb{D}_6$ action on U.

Any of these choices for U also have the save isotropy subgroups for the $\mathbb{D}_6 \times \mathbb{Z}_2$ action on U. Assume that Σ is an isotropy subgroup of this action. Therefore $\Sigma = \mathrm{Stab}(\mathbb{D}_6 \times \mathbb{Z}_2, u)$ for some $u \in U$. If $-1 \in \mathrm{Stab}(\mathbb{D}_6 \times \mathbb{Z}_2, u)$, then $-1 \cdot u = u$ which implies that $u = 0$ and $\mathrm{Stab}(\mathbb{D}_6 \times \mathbb{Z}_2, u) = \mathbb{D}_6 \times \mathbb{Z}_2$. For the $\mathbb{D}_6 \times \mathbb{Z}_2$ action on U where every subgroup of $\mathbb{D}_6$ is an isotropy subgroup, it can be shown that $\Sigma \lneq \mathbb{D}_6 \times \mathbb{Z}_2$ is an isotropy subgroup if, and only if, $-1 \notin \Sigma$. This result allows us to determine all of the isotropy subgroups for this group action by hand. We verified our calculations using GAP and the characterization in Equation (4.1) for the action of $\mathbb{D}_6 \times \mathbb{Z}_2$ on $U = \mathbb{R}^{12}$.

There are exactly 23 conjugacy classes of isotropy subgroups for the $\mathbb{D}_6 \times \mathbb{Z}_2$ action on $L_2(\Omega)$. Thus, a solution to the PDE (1.1) has one of 23 different symmetry types. The types are listed in 2.

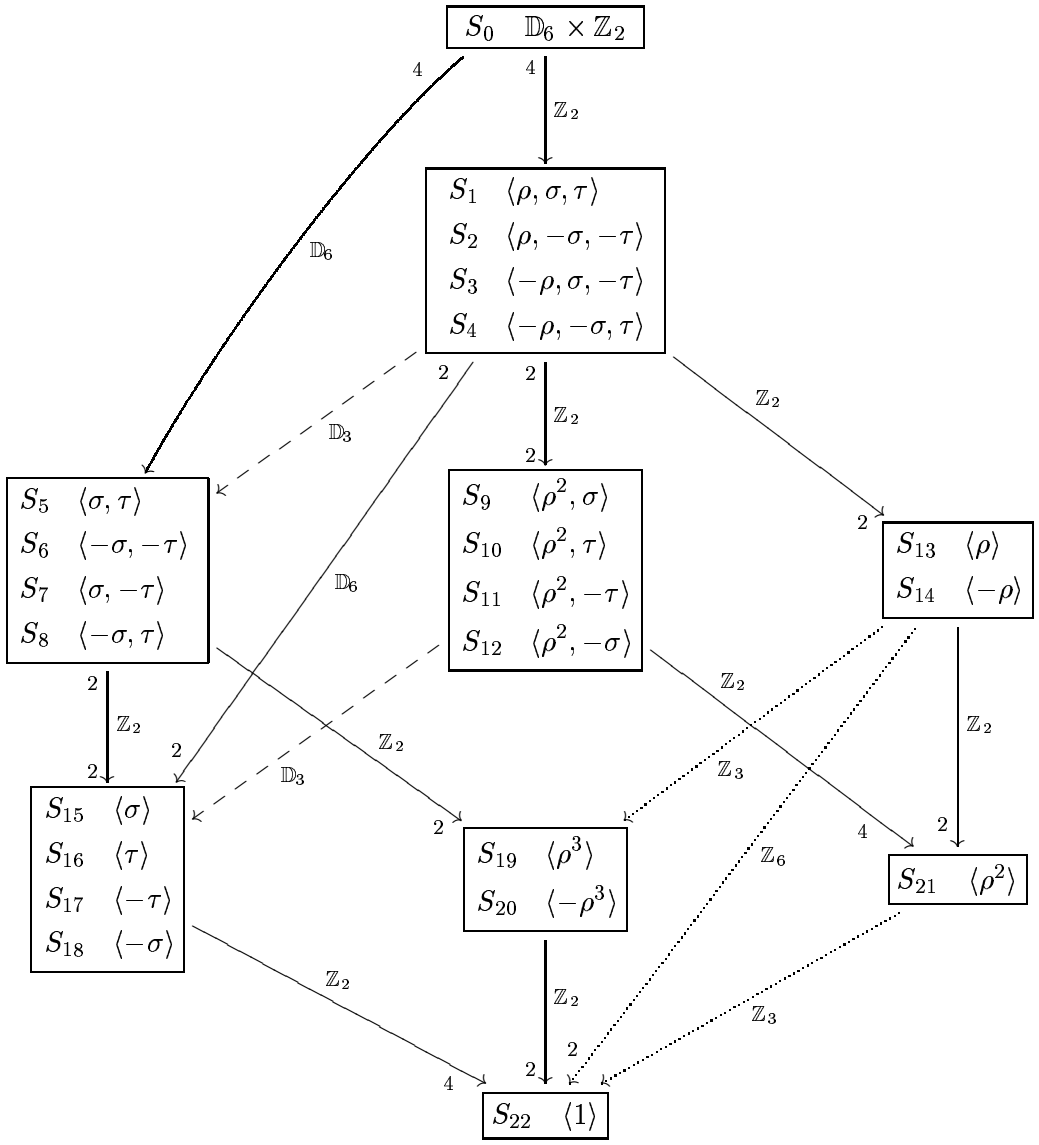

FIGURE 2. The reduced bifurcation digraph of symmetry types, which incorporates the well-known lattice of isotropy subgroups (see [7]). The vertices of the digraph are the equivalence classes of symmetry types. A name is given and a representative isotropy subgroup is indicated. Contour plots of solutions with each of these symmetry types are given in Figure 11 and Figure 12. The directed edges of the digraph are bifurcations with the indicated symmetry groups. A solid line denotes a pitchfork bifurcation, a dashed line is a transcritical bifurcation, and a dotted line is a more complicated bifurcation that is not predicted by the Equivariant Branching Lemma (EBL). The digraph is "reduced" because several edges from one box to another are identified: The small numbers on the edges tell the number of connections emanating from each symmetry type in a box. A missing small number means 1. The details of the edges from symmetry type S_2 are shown in Figure 3. digraph

The nonlinear PDE (1.1) can be written as $(\Delta + f)(u) = 0$, where $\Delta + f$ is a $\mathbb{D}_6 \times \mathbb{Z}_2$-equivariant operator. (There are subtleties due to the fact that the domain and range of Δ are different spaces. See [4] for a careful treatment.) In particular, $(\Delta + f)(-u) = -(\Delta + f)(u)$, since f is odd. As a consequence, if u is a solution to (1.1), then so is every element in its group orbit $(\mathbb{D}_6 \times \mathbb{Z}_2) \cdot u$. The Newton's method mapping is also $\mathbb{D}_6 \times \mathbb{Z}_2$-equivariant. We will describe later how this fact is exploited by our branch following code.

As a consequence of Propostion 4.2, we can solve the PDE (1.1), written as $(\Delta + f)(u) = 0$, by restricting u to functions in $\mathrm{Fix}_{L_2}(\Sigma)$. This leads to a simpler problem since the function space $\mathrm{Fix}_{L_2}(\Sigma)$ is simpler than L_2. An example of this is in Costa, Ding, and Neuberger [4]. The techniques of that paper, applied to our problem, would find solutions with Morse Index 2 within the space $\mathrm{Fix}(\mathbb{D}_6)$. Proposition (4.2) also implies to the GNGA, since the Newton iteration mapping is equivariant. If the initial guess is in a particular fixed point subspace, all the iterates will be in that fixed point subspace. Newton's method can converge to a solution with more, but not less, symmetry than the initial guess.

If we use a grid of level $\ell \geq 3$ to obtain the function space U then there exists a $\mathbb{D}_6$ orbit with 12 distinct grid points, then a subgroup $\Gamma \leq \mathbb{D}_6 \times \mathbb{Z}_2$ is an isotropy subgroup if and only if $(-1 \in \Gamma$ implies that $\Gamma = \mathbb{D}_6 \times \mathbb{Z}_2)$. In particular, the structure of isotropy subgroups is the same as that of the Γ_0 action on $L_2(\Omega)$.

We used a GAP [6] program and the level $\ell = 3$ grid G_{13} to find all the isotropy subgroups and the corresponding fixed point subspaces. The isotropy subgroups fall into 23 conjugacy classes.

For one isotropy subgroup from each symmetry type, $\Gamma_i \in S_i$, the GAP program also did all of the calculations necessary to classify the bifurcations of solutions with isotropy subgroup Γ_i. The bifurcation digraph in Figure 2 summarizes the results of those calculations. Figure 3 gives some of the details of the calculation for solutions with symmetry $\Gamma_2 = \langle \rho, -\sigma, -\tau \rangle \cong \mathbb{D}_6$.

Let us summarize how symmetry effects the eigenvalue equation (3.1). There are six $\mathbb{D}_6$-invariant subspaces in our decomposition of $\mathbb{R}^N = \bigoplus_{i=1}^{6} V^{(i)}$, corresponding to the six irreducible representations of $\mathbb{D}_6$ (see [20]). For the 2-dimensional irreducible representations of $\mathbb{D}_6$ ($i = 5$ and $i = 6$) the $\mathbb{D}_6$-invariant spaces can be further decomposed into spaces that are invariant under the Laplacian, even though they are not $\mathbb{D}_6$-invariant. Thus $V^{(5)} = V_1^{(5)} \oplus V_2^{(5)}$ and $V^{(6)} = V_1^{(6)} \oplus V_2^{(6)}$. For multiplicity-two eigenvalues of the Laplacian, the ARPACK program gave us two orthonormal eigenvectors in either $V^{(5)}$ or $V^{(6)}$ that do not respect this decomposition. In these cases we projected the eigenvectors onto the two Laplacian-invariant subsapces, for example $V_1^{(5)}$ and $V_2^{(5)}$, using the parities under x and y reflections. Hence, we give another set of names, $V_{p_x p_y d}$, to the 8 Laplacian-invariant spaces, where p_x and p_y describe the parity of the functions under the reflections σ and τ respectively, and d is the dimension of the associated irreducible representation, i.e., the multiplicity of the corresponding eigenvalue. Some calculations allow us to give simple descriptions of these Laplacian-invariant spaces:

v1-8 (4.5)

$$
\begin{aligned}
V_{++1} &:= V^{(1)} = \{u \in U \mid \rho \cdot u = u,\ \sigma \cdot u = u,\ \tau \cdot u = u\} \\
V_{--1} &:= V^{(2)} = \{u \in U \mid \rho \cdot u = u,\ \sigma \cdot u = -u,\ \tau \cdot u = -u\} \\
V_{+-1} &:= V^{(3)} = \{u \in U \mid \rho \cdot u = -u,\ \sigma \cdot u = u,\ \tau \cdot u = -u\} \\
V_{-+1} &:= V^{(4)} = \{u \in U \mid \rho \cdot u = -u,\ \sigma \cdot u = -u,\ \tau \cdot u = u\}
\end{aligned}
$$

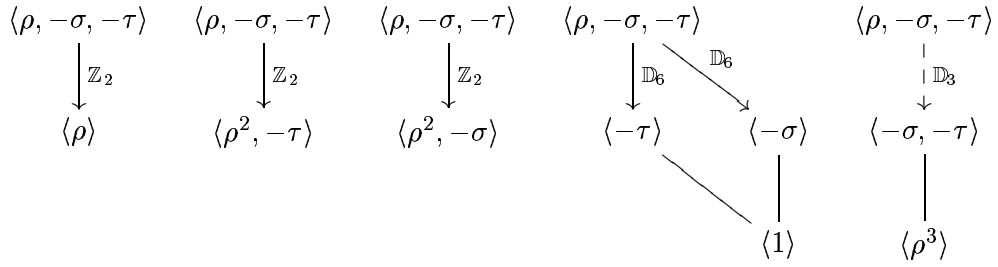

FIGURE 3. The five generic bifurcations of a solution with symmetry $\Gamma = \Gamma_2 = \langle \rho, -\sigma, -\tau \rangle \in S_2$. The five diagrams are the lattices of isotropy subgroups for the five nontrivial irreducible representations of $\mathbb{D}_6 \cong \Gamma$. An edge in the bifurcation digraph joins Γ to all maximal isotropy subgroups in each of the irreducible representations. The minimal isotropy subgroup of the i-th irreducible representation is the stabilizer of the critical eigenspace E_i at the bifurcation. The symmetry group of the bifurcation, $\Gamma/\operatorname{Stab}(E_i)$, is indicated as a label on the edge (either $\mathbb{Z}_2$, $\mathbb{D}_6$, or $\mathbb{D}_3$ in this example). This figure shows several details which are left out in Figure 2. For example, the submaximal isotropy subgroups are not indicated in Figure 2. Also, the identified arrows of the *reduced* bifurcation digraph shown separately here: The arrows from Γ to $\langle \rho^2, -\tau \rangle$ and to $\langle \rho^2, -\sigma \rangle$ are identified in Figure 2. Similarly, the arrows from Γ to $\langle -\tau \rangle$ and to $\langle -\sigma \rangle$ are identified in Figure 2. bif2

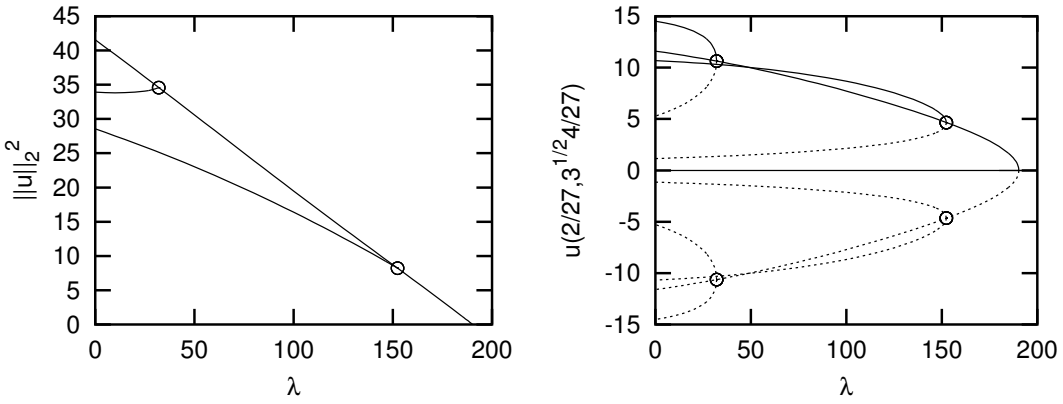

FIGURE 4. Bifurcation diagrams of the sixth primary branch, showing $||u||_2^2$ and $u(2/27, 4\sqrt{3}/27)$ as a function of λ. Since $||u||_2^2$ is a $\mathbb{D}_6 \times \mathbb{Z}_2$-invariant function of u, each conjugacy class of solution branches is shown as one curve. The disadvantage of plotting $||u||_2^2$ is that the curves are not well separated. The point $(2/27, 4\sqrt{3}/27)$ is not on any of the reflection axes of the snowflake region. There are 2 primary branches with symmetry S_1, four conjugate secondary branches with symmetry S_9, and four conjugate secondary branches with symmetry S_{10}. Our choice for the bifurcation diagrams in this paper combines the advantages of both views: $u(2/27, 4\sqrt{3}/27)$ is plotted as a function of λ for exactly one branch (the solid lines) from each conjugacy class. fig.verbose

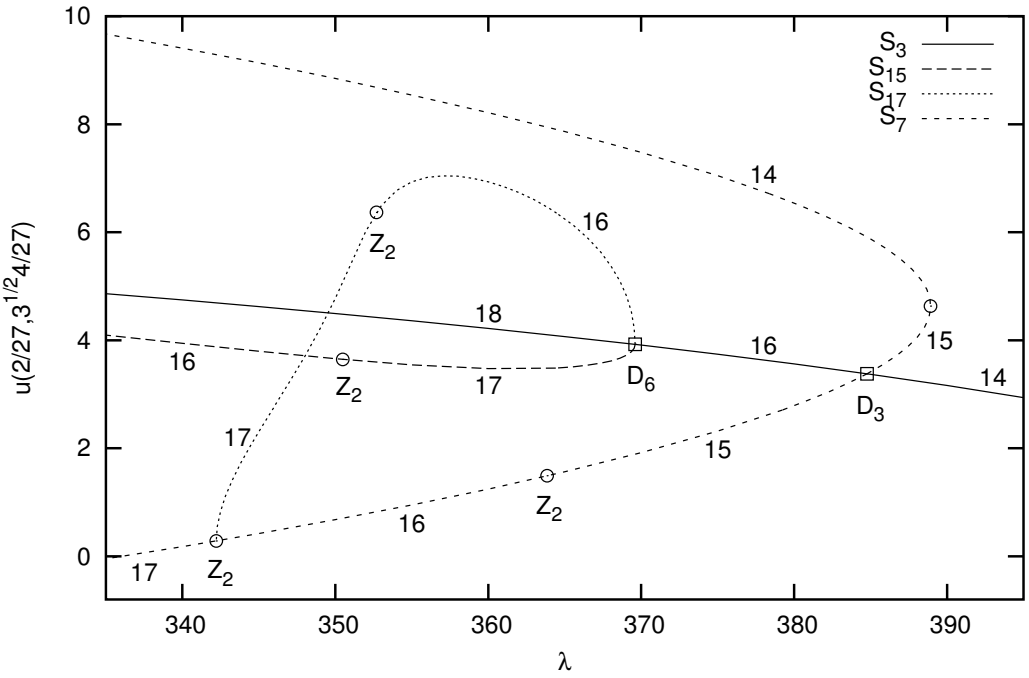

FIGURE 5. A partial bifurcation diagram of the 14-th primary branch showing a $\mathbb{D}_6$, a $\mathbb{D}_3$ and several $\mathbb{Z}_2$ bifurcations. At the $\mathbb{D}_6$ point, 12 branches of two different symmetry types bifurcate. At the $\mathbb{D}_3$ point, 6 branches of the same symmetry bifurcate. In accordance with Figure 4, only two branches need to be followed in both cases. For clarity, the branches bifurcating from 3 of the $\mathbb{Z}_2$ bifurcations are not followed. The numbers next to a branch indicate the MI of the solution. The MI changes by 2 at a square, and by 1 at a circle. fig.d3_d6

$$
\begin{aligned}
V^{(5)} &= \{u \in U \mid \rho^3 \cdot u = u,\ u + \rho^2 \cdot u + \rho^4 \cdot u = 0\} \\
V^{(6)} &= \{u \in U \mid \rho^3 \cdot u = -u,\ u + \rho^2 \cdot u + \rho^4 \cdot u = 0\} \\
V_{++2} := V_1^{(5)} &= \{u \in V^{(5)} \mid \sigma \cdot u = u,\ \tau \cdot u = u\} \\
V_{--2} := V_2^{(5)} &= \{u \in V^{(5)} \mid \sigma \cdot u = -u,\ \tau \cdot u = -u\} \\
V_{+-2} := V_1^{(6)} &= \{u \in V^{(6)} \mid \sigma \cdot u = u,\ \tau \cdot u = -u\} \\
V_{-+2} := V_2^{(6)} &= \{u \in V^{(6)} \mid \sigma \cdot u = -u,\ \tau \cdot u = u\}
\end{aligned}
$$

Contour plots of eigenfunctions with each of the eight symmetry types are shown in [20]. As we will see, this this decomposition of the function space is useful in the description of the symmetry types of solutions to (1.1).

Every fixed point subspace decomposes as a direct sum of the invariant spaces defined in (4.5). In fact, the possible symmetry types of the eigenfunctions of the Laplacian are $S_1, \ldots, S_8$. Because of this correspondence, the symmetry type of a solution $u \in U$ determines the possible nonzero

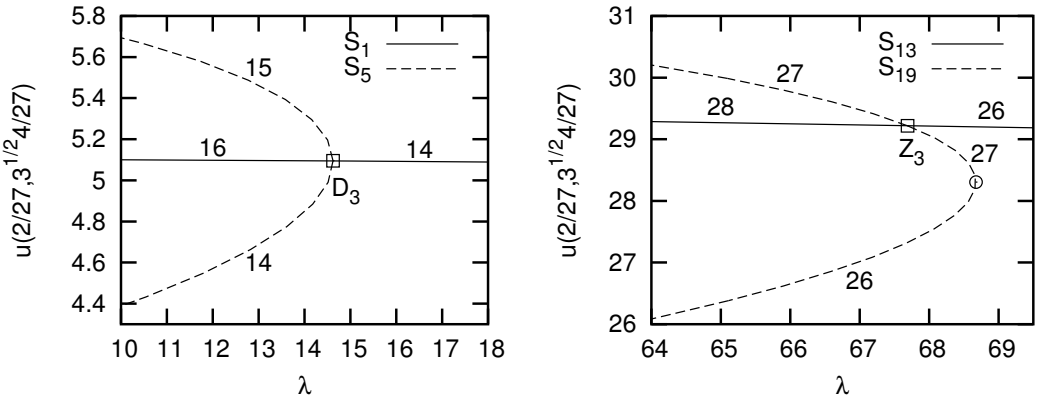

FIGURE 6. The $\mathbb{D}_3$-bifurcation of the 13-th primary branch (left). This is the only observed $\mathbb{D}_3$-bifurcation that is not transcritical. A $\mathbb{Z}_3$-bifurcation of a secondary branch of the 24-th primary branch (right). This bifurcation is not predicted by the EBL. The only remaining bifurcation symmetry type in Figure 2 is $\mathbb{Z}_6$. We only observed such a bifurcation with $M = 100$ modes. fig.d3b

coefficients of the expansion of u. For example, a solution with symmetry type S_{13} is a linear combination of eigenfunctions in $V^{(1)} \cup V^{(2)}$. We use this information to find solutions on bifurcating branches and to remain on a certain branch.

In our bifurcation diagrams we plot approximate solutions u evaluated at a generic point $(2/27, 4\sqrt{3}/27)$ versus the parameter λ; other choices for the vertical axis such as $J(u)$ or $\|u\|_\infty$ lead to less visible separation of branches. The generic point was chosen to be a common point on every level's grid, with a full $\mathbb{D}_6$ orbit. With this choice, solutions with different symmetry types are expected to have distinct and varying values on bifurcation diagrams. The points $(\lambda, 0)$ define the trivial branch, the only branch of symmetry type S_0. The branches bifurcating at eigenvalues of the Laplacian along the trivial branch are called primary branches and contain solutions with symmetry types $S_1, \ldots, S_8$. The digraph in Figure 2 explains the further *symmetry breaking* which occurs at secondary bifurcations.

5. Symmetry and Computational Efficiency

Several modifications of the GNGA (2.1) take advantage of symmetry to speed up the calculations. The fixed point subspace of the initial guess is computed. Suppose that there are M modes in our computation, but the dimension of $\mathrm{Fix}(\Sigma)$ is M_Σ. Only M_Σ of the M components of the gradient (2.2) are nonzero, so the numerical integrations are not done for the zero components. Furthermore, M_Σ^2 rather than M^2 numerical integrations are needed to compute the part of the Hessian matrix needed by the GNGA algorithm. (The numerical integration in (2.3) is done only if ψ_j and ψ_k are both in $\mathrm{Fix}(\Sigma)$. The $\lambda_j\, \delta_{jk}$term is included for all $j \in \{1, \ldots, M\}$ so that the Hessian is nonsingular.) We then solve the full linear system $h\chi = g$ with M equations and M unknowns. We could solve a reduced system with M_Σ equations and M_Σ unknowns, but this would not speed up the algorithm very much since the majority of the time is spent doing the numerical integrations. After Newton's method converges to a solution, the full Hessian needs to be calculated in order to

$\Gamma_0 = \mathbb{D}_6 \times \mathbb{Z}_2 \to$ $\mathrm{Fix}(\Gamma_0) = \{0\}$	Γ_1 $V^{(1)}$	Γ_2 $V^{(2)}$	Γ_2 $V^{(3)}$	Γ_4 $V^{(4)}$	Γ_5, Γ_6 $(\Gamma' = \Gamma_{19})$ $V^{(5)}$	Γ_7, Γ_8 $(\Gamma' = \Gamma_{20})$ $V^{(6)}$
					$\Gamma/\Gamma' \cong \mathbb{D}_6$ $N_\Gamma(\Sigma)/\Sigma \cong \mathbb{Z}_2$	$\Gamma/\Gamma' \cong \mathbb{D}_6$ $N_\Gamma(\Sigma)/\Sigma \cong \mathbb{Z}_2$

$\Gamma_1 = \langle \rho, \sigma, \tau \rangle \to$ $\mathrm{Fix}(\Gamma_1) = V^{(1)}$	Γ_{13} $V^{(2)}$	Γ_9 $V^{(3)}$	Γ_{10} $V^{(4)}$	Γ_5 $(\Gamma' = \Gamma_{19})$ $V^{(5)}$	Γ_{15}, Γ_{16} $(\Gamma' = \Gamma_{22})$ $V^{(6)}$
$\Gamma_2 = \langle \rho, -\sigma, -\tau \rangle \to$ $\mathrm{Fix}(\Gamma_2) = V^{(2)}$	Γ_{13} $V^{(1)}$	Γ_{11} $V^{(4)}$	Γ_{12} $V^{(3)}$	Γ_6 $(\Gamma' = \Gamma_{19})$ $V^{(5)}$	Γ_{17}, Γ_{18} $(\Gamma' = \Gamma_{22})$ $V^{(6)}$
$\Gamma_3 = \langle -\rho, \sigma, -\tau \rangle \to$ $\mathrm{Fix}(\Gamma_3) = V^{(3)}$	Γ_{14} $V^{(4)}$	Γ_9 $V^{(1)}$	Γ_{11} $V^{(2)}$	Γ_7 $(\Gamma' = \Gamma_{20})$ $V^{(6)}$	Γ_{15}, Γ_{17} $(\Gamma' = \Gamma_{22})$ $V^{(5)}$
$\Gamma_4 = \langle -\rho, -\sigma, \tau \rangle \to$ $\mathrm{Fix}(\Gamma_4) = V^{(4)}$	Γ_{14} $V^{(3)}$	Γ_{12} $V^{(2)}$	Γ_{10} $V^{(1)}$	Γ_8 $(\Gamma' = \Gamma_{20})$ $V^{(6)}$	Γ_{16}, Γ_{18} $(\Gamma' = \Gamma_{22})$ $V^{(5)}$
$\Gamma \cong \mathbb{D}_6$				$\Gamma/\Gamma' \cong \mathbb{D}_3$ $N_\Gamma(\Sigma)/\Sigma \cong \langle 1 \rangle$	$\Gamma/\Gamma' \cong \mathbb{D}_6$ $N_\Gamma(\Sigma)/\Sigma \cong \mathbb{Z}_2$

$\Gamma_5 = \langle \sigma, \tau \rangle \to$ $\mathrm{Fix}(\Gamma_5) = V^{(1)} \oplus V_1^{(5)}$	Γ_{19} $V^{(2)} \oplus V_2^{(5)}$	Γ_{15} $V^{(3)} \oplus V_1^{(6)}$	Γ_{16} $V^{(4)} \oplus V_2^{(6)}$
$\Gamma_6 = \langle -\sigma, -\tau \rangle \to$ $\mathrm{Fix}(\Gamma_6) = V^{(2)} \oplus V_2^{(5)}$	Γ_{19} $V^{(1)} \oplus V_1^{(5)}$	Γ_{18} $V^{(4)} \oplus V_2^{(6)}$	Γ_{17} $V^{(3)} \oplus V_1^{(6)}$
$\Gamma_7 = \langle \sigma, -\tau \rangle \to$ $\mathrm{Fix}(\Gamma_7) = V^{(3)} \oplus V_1^{(6)}$	Γ_{20} $V^{(4)} \oplus V_2^{(6)}$	Γ_{15} $V^{(1)} \oplus V_1^{(5)}$	Γ_{16} $V^{(2)} \oplus V_2^{(5)}$
$\Gamma_8 = \langle -\sigma, \tau \rangle \to$ $\mathrm{Fix}(\Gamma_8) = V^{(4)} \oplus V_2^{(6)}$	Γ_{20} $V^{(3)} \oplus V_1^{(6)}$	Γ_{18} $V^{(2)} \oplus V_2^{(5)}$	Γ_{17} $V^{(1)} \oplus V_1^{(5)}$
$\Gamma \cong \mathbb{Z}_2 \times \mathbb{Z}_2$			

TABLE 3. The 64 generic symmetry-breaking bifurcations. This Table and the next show the results that are summarized in the reduced bifurcation digraph, Figure 2. For each isotropy subgroup Γ_i, the first row shows the symmetry of the solutions created at the bifurcations. The second row shows the the isotypic decomposition $U = \bigoplus_j V_{\Gamma_i}^{(j)}$ of the Γ_i action on U. Barring accidental degeneracy, the critical eigenspace E lies in one of the $V_{\Gamma_i}^{(j)}$ components. The maximal (proper) isotropy subgroup, Σ, and the minimal isotropy subgroup, Γ', of the Γ_i action on $V_{\Gamma_i}^{(j)}$ are computed by GAP. Thus, $\Gamma_i = \Gamma \gneqq \Sigma \geq \Gamma'$. Branches with Σ symmetry, listed after the arrow, are known to bifurcate in a gradient system such as ours. The minimal isotropy subgroup, Γ', is listed if it is not the same as Σ. The symmetry group of the bifurcation, Γ/Γ', is listed if it is not $\mathbb{Z}_2$. If $\Sigma \neq \Gamma'$, the symmetry of the PDE restricted to $\mathrm{Fix}(\Sigma)$, namely $N_\Gamma(\Sigma)/\Sigma$, is listed. The pitchfork bifurcations, with symmetry group $\Gamma/\Gamma' = \mathbb{Z}_2$ have a one-dimensional critical eigenspace. The others, for which Γ/Γ' is listed, have $\dim(E) = 2$, indicating that the Morse Index of the base solution changes by 2 at the bifurcation. Most of the bifurcating solutions have $\dim(\mathrm{Fix}_E(\Sigma)) = 1$, indicating that the EBL holds, and it is easy to follow the bifurcating branch by choosing a perturbation with a critical eigenvector with isotropy Σ. Table 4 indicates the bifurcations where $\dim(\mathrm{Fix}_E(\Sigma)) = 2$. In these cases no critical eigenvector has more symmetry that the others, and the EBL does not hold. Nevertheless, in gradient systems solution branches with the maximal isotropy Σ are created at the bifurcation.

bifTableA

$\Gamma_9 = \langle \rho^2, \sigma \rangle \to$ $\mathrm{Fix}(\Gamma_9) = V^{(1)} \oplus V^{(3)}$	Γ_{21} $V^{(2)} \oplus V^{(4)}$	$\Gamma_{15}\ (\Gamma' = \Gamma_{22})$ $V^{(5)} \oplus V^{(6)}$
$\Gamma_{10} = \langle \rho^2, \tau \rangle \to$ $\mathrm{Fix}(\Gamma_{10}) = V^{(1)} \oplus V^{(4)}$	Γ_{21} $V^{(2)} \oplus V^{(4)}$	$\Gamma_{16}\ (\Gamma' = \Gamma_{22})$ $V^{(5)} \oplus V^{(6)}$
$\Gamma_{11} = \langle \rho^2, -\tau \rangle \to$ $\mathrm{Fix}(\Gamma_{10}) = V^{(3)} \oplus V^{(2)}$	Γ_{21} $V^{(4)} \oplus V^{(2)}$	$\Gamma_{17}\ (\Gamma' = \Gamma_{22})$ $V^{(6)} \oplus V^{(5)}$
$\Gamma_{12} = \langle \rho^2, -\sigma \rangle \to$ $\mathrm{Fix}(\Gamma_{12}) = V^{(4)} \oplus V^{(2)}$	Γ_{21} $V^{(3)} \oplus V^{(1)}$	$\Gamma_{18}\ (\Gamma' = \Gamma_{22})$ $V^{(6)} \oplus V^{(5)}$
$\Gamma \cong \mathbb{D}_3$		$\Gamma/\Gamma' \cong \mathbb{D}_3$ $N_\Gamma(\Sigma)/\Sigma \cong \langle 1 \rangle$

$\Gamma_{13} = \langle \rho \rangle \to$ $\mathrm{Fix}(\Gamma_{13}) = V^{(1)} \oplus V^{(2)}$	Γ_{21} $V^{(3)} \oplus V^{(4)}$	Γ_{19} $V^{(5)}$	Γ_{22} $V^{(6)}$
$\Gamma_{14} = \langle -\rho \rangle \to$ $\mathrm{Fix}(\Gamma_{14}) = V^{(4)} \oplus V^{(3)}$	Γ_{21} $V^{(2)} \oplus V^{(1)}$	Γ_{20} $V^{(6)}$	Γ_{22} $V^{(5)}$
$\Gamma \cong \mathbb{Z}_6$		$\Gamma/\Gamma' \cong \mathbb{Z}_3$ $N_\Gamma(\Sigma)/\Sigma \cong \mathbb{Z}_3$ $\dim \mathrm{Fix}_E(\Sigma) = 2$	$\Gamma/\Gamma' \cong \mathbb{Z}_6$ $N_\Gamma(\Sigma)/\Sigma \cong \mathbb{Z}_6$ $\dim \mathrm{Fix}_E(\Sigma) = 2$

$\Gamma_{15} = \langle \sigma \rangle \to$ $\mathrm{Fix}(\Gamma_{15}) = V^{(1)} \oplus V^{(3)} \oplus V_1^{(5)} \oplus V_1^{(6)}$	Γ_{22} $V^{(4)} \oplus V^{(2)} \oplus V_2^{(6)} \oplus V_2^{(5)}$
$\Gamma_{16} = \langle \tau \rangle \to$ $\mathrm{Fix}(\Gamma_{16}) = V^{(1)} \oplus V^{(4)} \oplus V_1^{(5)} \oplus V_2^{(6)}$	Γ_{22} $V^{(3)} \oplus V^{(2)} \oplus V_1^{(6)} \oplus V_2^{(5)}$
$\Gamma_{17} = \langle -\tau \rangle \to$ $\mathrm{Fix}(\Gamma_{17}) = V^{(3)} \oplus V^{(2)} \oplus V_1^{(6)} \oplus V_2^{(5)}$	Γ_{22} $V^{(1)} \oplus V^{(4)} \oplus V_1^{(5)} \oplus V_2^{(6)}$
$\Gamma_{18} = \langle -\sigma \rangle \to$ $\mathrm{Fix}(\Gamma_{18}) = V^{(4)} \oplus V^{(2)} \oplus V_2^{(6)} \oplus V_2^{(5)}$	Γ_{22} $V^{(1)} \oplus V^{(3)} \oplus V_1^{(5)} \oplus V_1^{(6)}$
$\Gamma \cong \mathbb{Z}_2$	

$\Gamma_{19} = \langle \rho^3 \rangle \to$ $\mathrm{Fix}(\Gamma_{19}) = V^{(1)} \oplus V^{(2)} \oplus V^{(5)}$	Γ_{22} $V^{(3)} \oplus V^{(4)} \oplus V^{(6)}$
$\Gamma_{20} = \langle -\rho^3 \rangle \to$ $\mathrm{Fix}(\Gamma_{20}) = V^{(4)} \oplus V^{(3)} \oplus V^{(6)}$	Γ_{22} $V^{(2)} \oplus V^{(1)} \oplus V^{(5)}$
$\Gamma \cong \mathbb{Z}_2$	

$\Gamma_{21} = \langle \rho^2 \rangle \to$ $\mathrm{Fix}(\Gamma_{21}) = V^{(1)} \oplus V^{(3)} \oplus V^{(4)} \oplus V^{(2)}$	Γ_{22} $V^{(5)} \oplus V^{(6)}$
$\Gamma \cong \mathbb{Z}_3$	$\Gamma/\Gamma' \cong \mathbb{Z}_3$ $N_\Gamma(\Sigma)/\Sigma \cong \mathbb{Z}_3$ $\dim \mathrm{Fix}_E(\Sigma) = 2$

bifTableB

TABLE 4. Continuation of Table 3.

compute the MI. Here, too, we can take advantage of the symmetry. Since h is a Σ-equivariant operator, $h_{jk} = 0$ if ψ_j and ψ_k are in different subspaces of the decomposition into h invariant spaces $V_j^{(i)}$ of the Σ action on U. In other words, the Hessian is block diagonal in the isotypic decomposition of the Σ action on U.

For example, the symmetry type $\Sigma = \mathbb{D}_6 \in S_1$ has $M_\Sigma = 30$ when $M = 300$. When all of the 90300 numerical integrations were done it took about 44 seconds to do one iteration of Newton's method. With the symmetry improvements it takes about 1.5 seconds per Newton iteration, and then about 11 seconds to compute the full Hessian and the Morse index.

6. Automated Branch Following and Symmetry.

branch_section

The branch following code is a complex collection of about a dozen Perl scripts, Mathematica and Gnuplot scripts and a C++ program. These programs write and call each other fully automatically and communicate through output files, pipes and command line arguments. A complete bifurcation diagram can be produced by a single call to the main Perl script.

The C++ program implements the GNGA algorithm. Its input is a vector of coefficients $a \in \mathbb{R}^M$ for an initial guess in Newton's method, an interval for λ, a stepsize for λ and several other parameters such as the level and the number of modes used in the expansion of solutions. It finds solutions on a single branch of the bifurcation diagram. Every solution is written as a single line in an output file. This line contains all the information about the solution such as the level, the number of modes, the symmetry of the solution, the stepsize, etc. Each line in the output file can be used to write an input file for a later call to the C++ program.

The C++ program has a main branch that it finds at a starting λ using the supplied coefficients as a guess for Newton's method. It attempts to follow this branch all the way to the final λ, usually 0. Heuristics are used to double or halve the λ stepsize when needed, keeping the stepsize in the interval from the initial stepsize (input to the C++ program) to the initial stepsize over 32. For example, the stepsize is halved if Newton's method does not converge, if it converges to a solution with the wrong symmetry, or if more than one bifurcation is detected in one λ step.

The Morse index is computed at each λ value on the main branch. When the MI changes a subroutine is called to handle the bifurcation before the main branch is continued. If the MI changes from m_1 to m_2, we define $m = \max\{m_1, m_2\}$. Then the bifurcation point is approximated by using the secant method to set the m-th eigenvalue of the Hessian $h(u)$ to zero as a function of λ. The GNGA is needed at each step of the secant method to compute $u = u(\lambda)$. We find that the GNGA works well even though we are approximating a solution for which the Hessian is singular.

I'm not sure I improved over the old version

At a Morse index change the code adjusts the λ stepsize to determine the number of bifurcation points stepped over. For each bifurcation point, the secant method is applied to find the value of λ making the appropriate near zero eigenvalues of the Hessian critical within tolerance; Newton's method is used at each secant iteration to get a new approximation of the bifurcation point and calculate the new near critical eigenvalues.

After the bifurcation point is approximated, a short segment of each bifurcating branch is computed and one output file is written for each branch. If the Equivariant Branching Lemma (EBL) holds then we know exactly which critical eigenvector to use for each branch. Let the Fourier coefficients of the solution at the bifurcation point be a^*, let the normalized critical eigenvector be $e \in \mathbb{R}^M$, and let k be defined by $|e_k| \geq |e_i|$ for all i. We then use the pmGNGA with the initial guess

$a = a^* + t\,e$, keeping the k-th component fixed and solving for λ and the other $M-1$ components of a. We start with $t = 0.1$, but this is decreased if Newton's method does not converge. More points on the bifurcating branch are computed in the same way, except that a^* is the last solution found on the branch. This short segment of the bifurcating branch ends when λ reaches the bifurcation value λ^* minus the stepsize, or when the pmGNGA does not converge even when t is extremely small, or when a maximum number of points on the branch is computed.

follow_branch *Algorithm* 6.1. (`follow_branch`)

(1) Input: bifurcation point (λ, a), one critical eigenvector $e \in \mathbb{R}^M$ and a stepsize $\Delta\lambda < 0$. The subroutine writes a file with the first part of a bifurcating branch.
(2) Write (λ, a) to output file. Set $t = 0.1$. Set $\lambda_b = \lambda$.
(3) Compute index k so that $|e_k| \geq |e_i|$ for all $i \in \{1, \ldots, M\}$.
(4) Repeat until $\lambda_b - \lambda < \Delta\lambda$, or $t < 0.1/32$ or some maximum number of points have been written to the file.
    (a) Do the pmGNGA with initial guess $(\lambda, a + t\,e)$, fixing coefficient k.
    (b) If Newton's method converges replace (λ, a) by the solution found and write this point to the file, else $t \leftarrow t/2$

Note that the pmGNGA can follow a branch that bifurcates to the right or the left. Those that bifurcate to the right usually turn over in a saddle-node "bifurcation" that does not offer any difficulty for the pmGNGA. Some numerical methods use a Liapunov-Schmidt reduction, but our method does not need to do this.

In the bifurcations with $\mathbb{Z}_3$ and $\mathbb{Z}_6$ symmetry in our problem, the EBL does not hold: The 2-dimensional critical eigenspace does not have a one-dimensional subspace with more symmetry. We handled this case with some heuristics. We plan to extend our code to problems with arbitrary (finite) symmetry groups. In the general code we will check for bifurcating solutions that are not predicted by the EBL by applying the pmGNGA with random (normalized) critical eigenvectors repeatedly until it appears that all equivalence classes of solutions have been found.

The branch following code is called recursively by a main Perl script. Initially the C++ program follows the trivial branch on a given λ range. This results in an output file for the trivial branch and another output file for each bifurcating primary branch. Then the short parts of the primary branches are followed with more calls to the C++ program. Any bifurcating branch results in a new output file, and the Perl script makes another call to the C++ program to continue that branch. The main Perl script's most important job is book keeping. It saves the output files with distinct names, and calls the branch following code to continue each of the new branches. The process stops when all the branches are fully followed.

In this way, a complete bifurcation diagram is produced by a single invocation of the main Perl script. There is no need to guess initial conditions for input to Newton's method, since the trivial solution is known exactly ($a = 0$) and all the other solutions are followed automatically.

The main Perl script calls several other smaller scripts. For example, there is a script which extracts solutions from output files and feeds them to the branch following code as input. Another script creates Gnuplot scripts on the fly to generate bifurcation diagrams. Branch following results in a great number of output files. The organization is an important task. Perl scripts are used to automatically number and store the output files and create human readable reports about them.

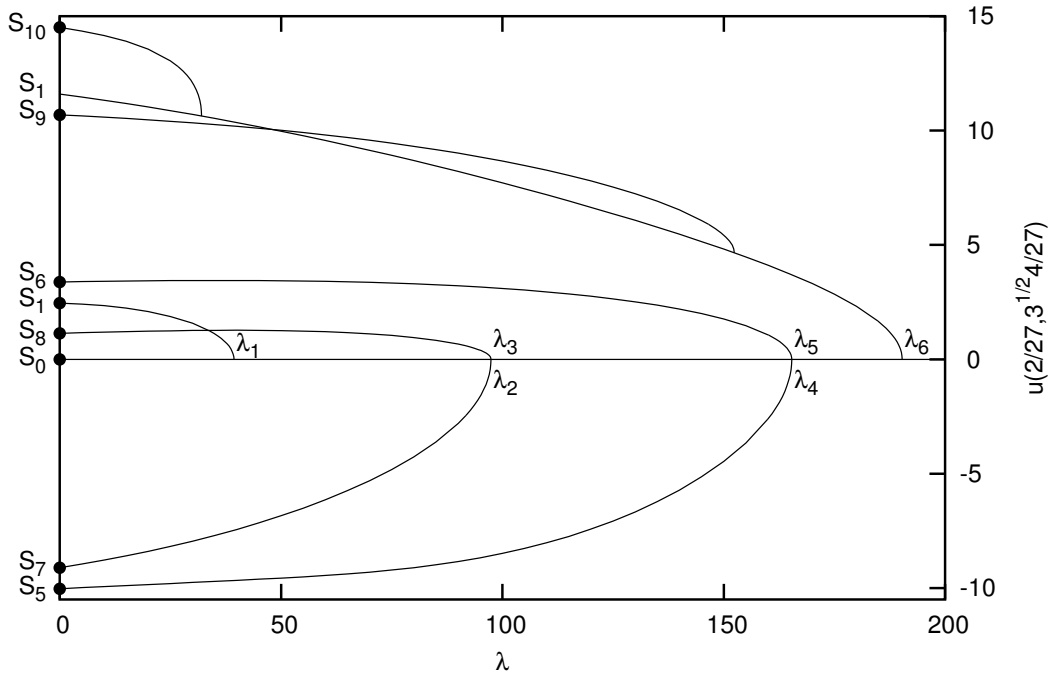

FIGURE 7. The complete bifurcation diagram for the first six primary branches bifurcating from the trivial branch. Primary branch j is labeled by the eigenvalue λ_j at which it bifurcates. The j-th primary branch has MI j near the bifurcation. The second branch, with symmetry S_7, contains the CCN solution. The dots at $\lambda = 0$ in Figures 7–10 correspond to solutions depicted in Figures 11 and 12. We used the level 5 grid with 300 modes in creating all bifurcation diagrams. In Figure 15 convergence data for the solution of symmetry type S_{10} at $\lambda = 0$ is provided. bif1-6

7. Numerical Results.

Our goal was to find solutions to (1.1) at $\lambda = 0$ with all 23 symmetry types. The 24-th branch is the first one with symmetry type S_2, so we followed the first 24 primary branches. With level $\ell = 5$ and $M = 300$ modes, which gave our most accurate results, this found solutions with all symmetry types except S_{11} and S_{14}. We then searched the first 100 primary branches, only following solutions with symmetry above S_{11} and S_{14} on the bifurcation digraph (Figure 2.) In this way we found solutions with all 23 symmetry types. The bifurcation diagrams which lead to these solutions are shown in Figures 7–10. We chose one solution at $\lambda = 0$ with each symmetry type by taking the one descended from the lowest primary branch. These choices are indicated by dots in Figures 7–10, and the corresponding contour diagrams of the solutions are shown in Figures 11 and 12. The contour diagrams use white for $u > 0$ and black for $u < 0$, and gray indicates $u = 0$. Equally spaced contours are drawn along with dots for local extrema. Details about these contour diagrams are found in [20].

At level $\ell = 5$ we have computed 300 eigenfunctions so $M \leq 300$ is possible. At level $\ell = 6$ we computed only 100 eigenfunctions. Due to our limited computational resources, using more than 100

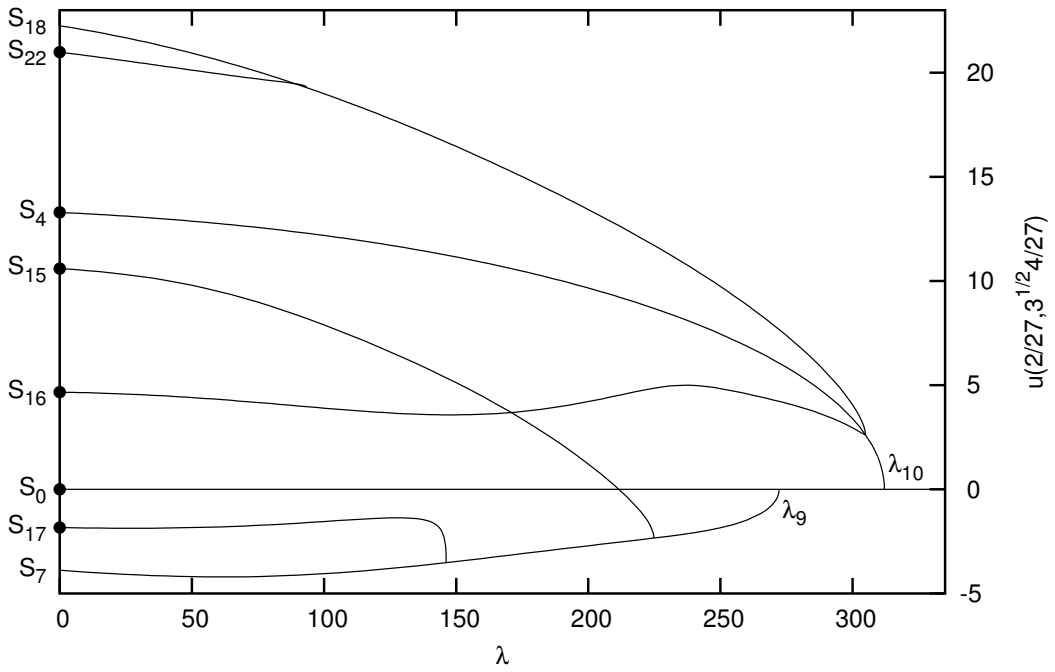

FIGURE 8. A partial bifurcation diagram showing some of the solutions bifurcating from the 9-th and 10-th primary branches. Again, the dots at $\lambda = 0$ indicate solutions shown in Figures 11 and 12. bifB

modes on level 6 was not practical. We ran a small subset of our experiments using a range of modes and levels in order to observe convergence and qualitative stability of the implementation of our algorithm. In Figure 13 we fix $\ell = 5$ and plot the sixth branch for $M \in \{100, 200, 300\}$. In Figure 14 we fix $M = 100$ and plot the same branch for $\ell \in \{4, 5, 6\}$. By definition, this branch bifurcates from the trivial solution at λ_6. Since our approximation to this eigenvalue depends on the level, it is expected that the approximate branches emanate from the same point in Figure 13, but from slightly different points in Figure 14. Also note that in Figure 14 the level 5 and 6 approximations are virtually indistinguishable. This indicates that with the results with $(\ell, M) = (5, 300)$ are more accurate than those with $(6, 100)$. Based on this and other similar convergence results, we chose to use level 5 with 300 modes in most of our numerical experiments. With these parameters, each step of Newton's method took from 1.5 to 44 seconds, depending on the symmetry of the solution.

In Figure 15 we present a visualization of the joint effects of the number modes and grid points on the approximation of the solution with S_{10} symmetry on the this sixth branch at $\lambda = 0$. The horizontal segments of the graphs correspond to the addition of modes with zero coefficients for this solution. Notice that the level 4 graph crosses the levels 5 and 6 graphs between modes 50 and 51, and back again between modes 51 and 52. In fact, on level 4 the eigenfunction corresponding to λ_{51} has symmetry type S_1 while on levels 5 and 6 this eigenfunction has symmetry type S_4. Similarly, the symmetry type of the eigenfunction corresponding to λ_{52} switches from S_4 to S_1 when the level is increased from 4 to 5.

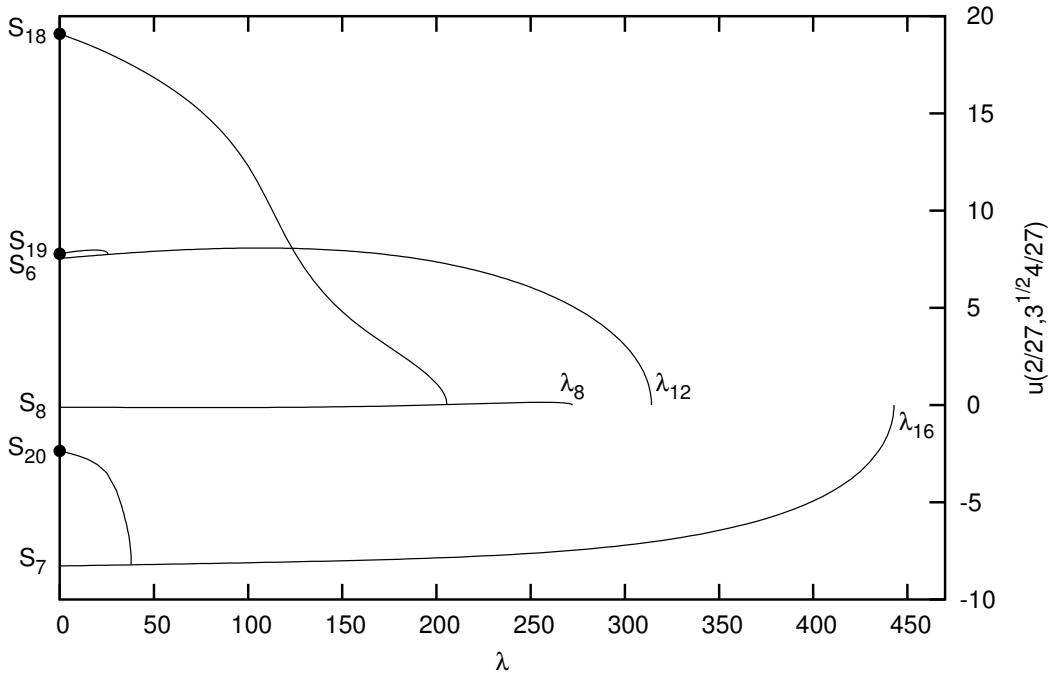

FIGURE 9. A partial bifurcation diagram providing three additional symmetry types. For clarity, the trivial branch is not shown in this and the next figure. bifC

8. MPA

We first briefly summarize the results from [2] and [4], and then prove the existence of several solutions to our specific problem via mountain pass type arguments. Of interest to those seeking to prove the existence of still more solutions, we also observe the existence numerically of other solutions using mountain pass type algorithms.

Let W be the well-studied Nehari manifold $W = \{u \neq 0 : J'(u)(u) = 0\}$, and W_1 be its subset $\{u \in W : u_+, u_- \in W\}$ (where $u_+(x) = \max\{u(x), 0\}$ and $u_- = \min\{u(x), 0\}$). In [1], and later in [2], the mountain pass theorem was applied to the functional J for a class of superlinear/subcritical nonlinearites f to obtain the existence of a pair of one-sign solutions, positive and negative respectively. These solutions can be characterized as global and/or local minima of $J|_W$. In [5], and later in [17], the mountain pass algorithm (MPA) was developed. The algorithm follows the corresponding constructive existence proof and finds these solutions numerically by performing (Sobolev) gradient descent constrained to W. In [2] the existence of a sign-changing solution to the same class of superlinear/subcritical problems was found by minimizing J_{W_1}. Again in [17], the MPA was extended to find this sign-changing solution. Essentially, ray projections of the positive and negative parts are used to gain membership to W_1, whereby again steepest descent is used. In [4], this method was termed the "modified mountain pass algorithm" (MMPA). In that work, both the sign-changing existence proof from [2] and the MMPA were extended to find solutions with symmetry on symmetric domains.

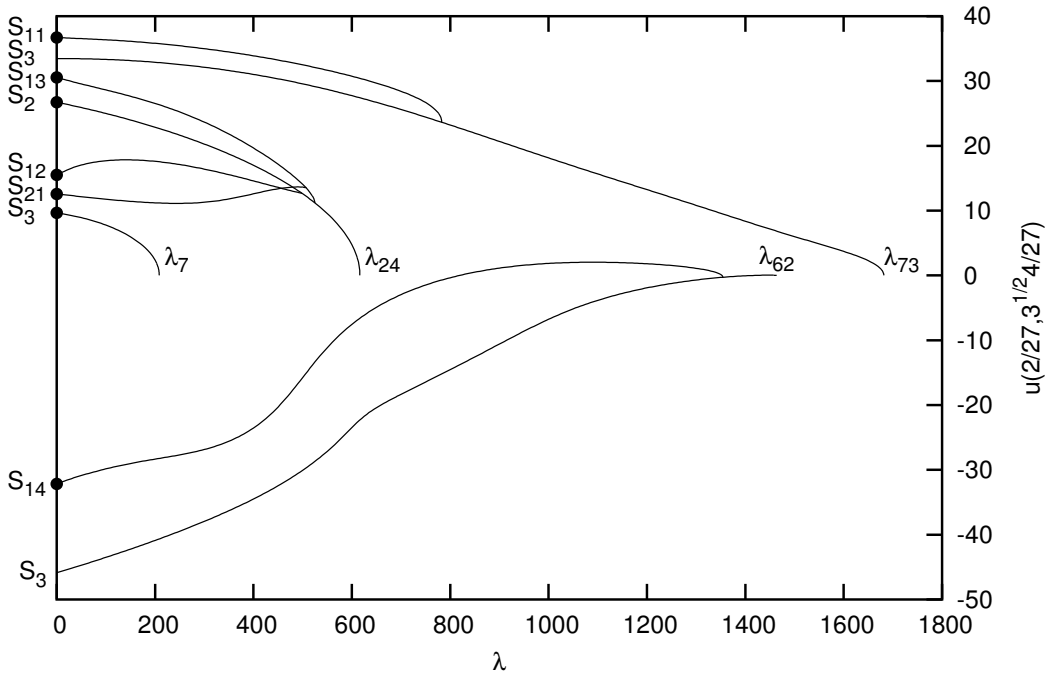

FIGURE 10. A partial bifurcation diagram containing solutions of the seven remaining symmetry types. Primary branch 24 is the first branch with symmetry type S_2. The symmetry types S_{14} and S_{11} were found by searching the first one hundred primary branches, following only those branches which can lead to solutions with the desired symmetry. These two solutions are included for completeness, but their existence for the PDE would have to be confirmed with more modes and a higher level approximation of the eigenfunctions. bifD

Specifically, the existence theorem in [4] assumes that there is a unitary representation $\{T(k)\}_{k\in G}$ of a compact topological group G, that the corresponding fixed point subspace $\mathrm{Fix}(G)$ is nontrivial and closed by the taking of positive and negative parts, and that J is invariant under the representation: $J(T(k)u) = J(u)$ for all $u \in H$ and $k \in G$. As a result, it is shown that there exists a sign-changing solution in $\chi = \mathrm{Fix}(G)$.

Several facts are clear. One, the finite dimensional group-theoretic vector results in the present paper as applied to the grid certainly translate to the inifinite dimensional function setting. That is to say, each of our 21 nontrival symmetry types provides such a setting. Secondly, the averaging used in the MMPA in [4] to gain membership to the invariant subspace $\mathrm{Fix}(G)$ is a specific application of our theoretical projection techniques; Our eigenfunction decompostion and corresponding symmetry analysis makes this process now particularly easy. Also, the proof can be easily adpated to the (unmodified) mountain pass setting; while originally used to obtain one-sign solutions, if a given isotropy group inherently implies that the invariant space contains sign-changing elements then minimization of $J|_{\chi\cap W}$ will yield sign-changing solutions.

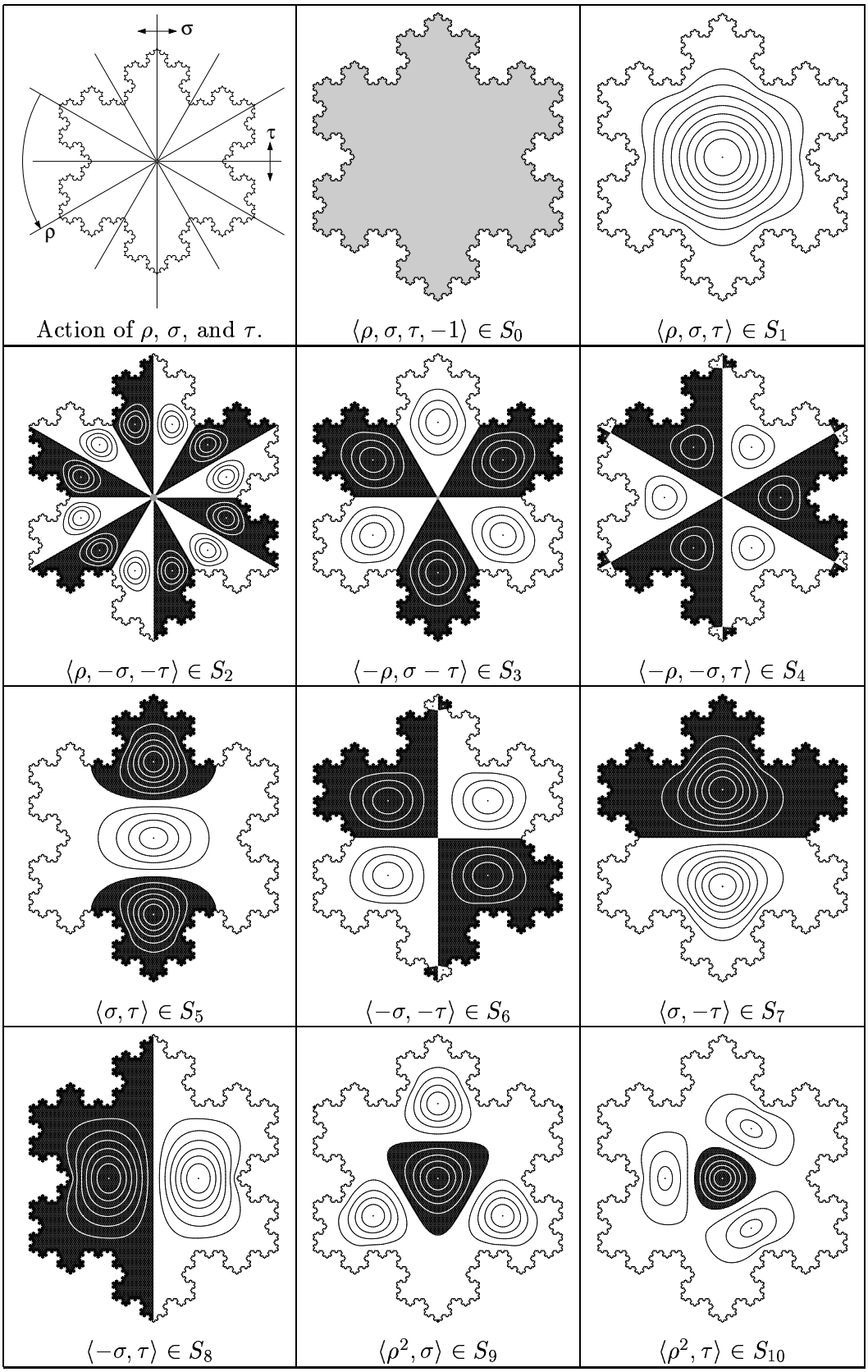

FIGURE 11. The action of the generators of $\mathbb{D}_6$ on the plane, along with contour plots of solutions with symmetry types $S_0, \ldots, S_{10}$ at $\lambda = 0$. sols1

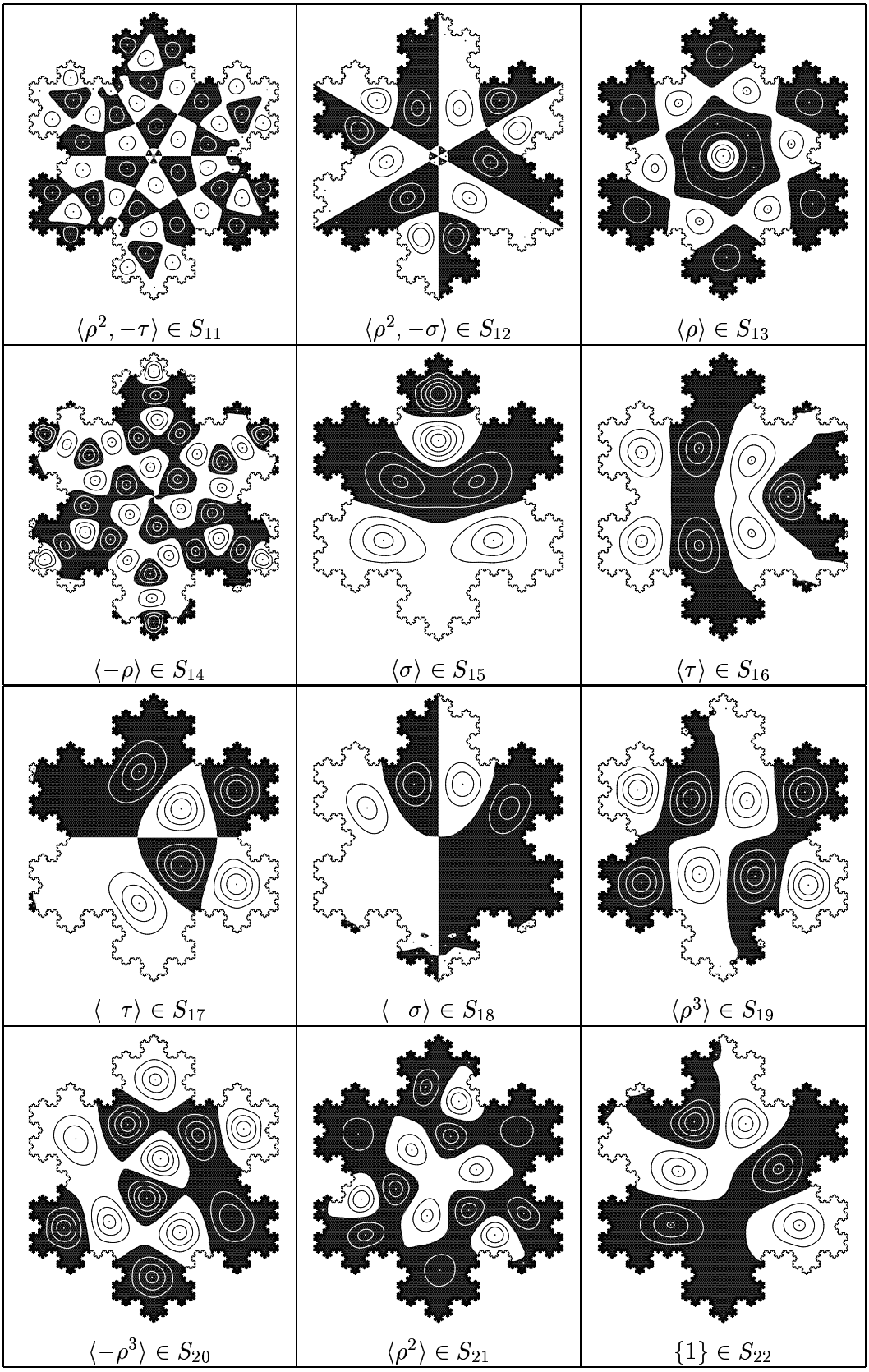

FIGURE 12. Contour plots of solutions with symmetry types $S_{12}, \ldots, S_{22}$ at $\lambda = 0$. sols2

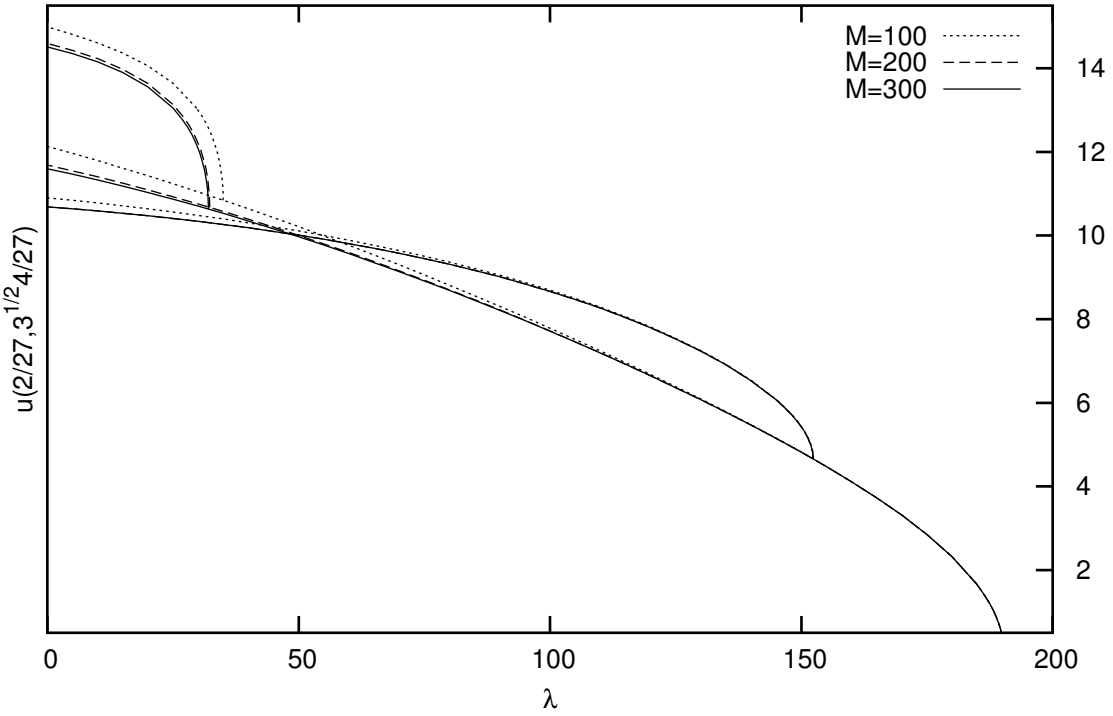

FIGURE 13. The sixth branch from Figure 7 plotted for level $\ell = 5$, $M \in \{100, 200, 300\}$ modes. biflim1

When minimizing $J|_{\chi \cap W}$ or $J|_{\chi \cap W_1}$, it may be that the solution obtained is the same one as another for a different invariant subspace further down the lattice corresponding to an isotropy subgroup of the isotropy subgroup for χ. Hence, for our region and an odd nonlinearity f such as the one used in our experiments, we can only prove that there exists a positive and negative solution of symmetry type S_1, and pairs $(\pm)$ of sign-changing solutions of symmetry types S_1, S_2, S_3, and S_4. The MI 1 one-sign solutions can be approximated by using the MPA on $J|_{S \cap \chi}$ for $\chi = \mathrm{Fix}(\langle \rho, \sigma \rangle)$. The sign-changing solutions correpsonding to that symmetry use the MMPA on $J|_{S \cap \chi}$. For symmetry types S_2, S_3, and S_4 there is no difference between applying the MPA and the MMPA, since members of the correpsonding invariant spaces are necessarily sign-changing anyway. Beyond these 10 nontrivial solutions, we cannot prove the existence of more solutions with symmetry using solely this technique. It seems that there should be a higher MI modification of the MMPA that uses positive and negative parts of u restricted to sectors of Ω, but we have not yet investigated this idea. Experimentally, we did obtain more sign-changing solutions with symmetry by applying the MPA and MMPA to each of the 21 invariant subspaces, although we did indeed frequently find redundant solutions when working in spaces lower in the lattice. In Table 8 we show the results of applying the MPA and MMPA to each of the subspaces; approximate solutions so obtained were fed into the GNGA in order to verify correctness and more importantly, to compute the MI. All included experiments were for $\lambda = f'(0) = 0$, where the manifold W is nondegenerate. Necessarily, when the group involves negation or the MMPA is used, the solution is sign-changing;

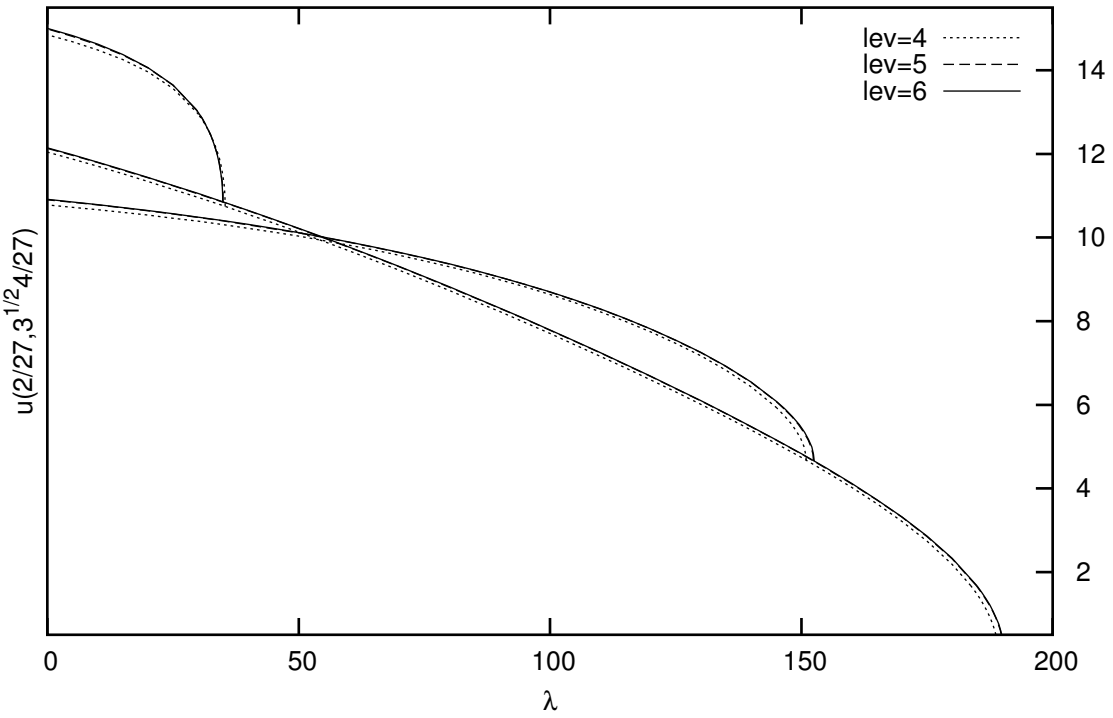

FIGURE 14. The sixth branch from Figure 7 plotted for levels $\ell \in \{4, 5, 6\}$, $M = 100$ modes. biflim2

for groups without negation where the MPA is used, only the (apparently unique) positive and negative one-sign solutions of MI 1 and symmetry type S_2 were found. The MI 2 sign-changing solutions of symmetry type S_8 are the "CCN" solutions from [2]; The MI 8 sign-changing solutions of symmetry type S_2 are the "radially symmetric" ones discussed in [4].

9. Conclusions.

References

ar [1] Ambrosetti and Rabinowitz, *Dual ...*

ccn [2] Castro, A., J. Cossio and J. M. Neuberger, *Sign-Changing Solutions for a Superlinear Dirichlet Problem*, Rocky Mnt. J. Math **27** (1997), no. 4, p1041-1053.

cdn2 [3] Castro, A., P. Drabek and J. M. Neuberger, *Sign-Changing Solutions for a Superlinear Dirichlet Problem, II*, Proceedings of the Fifth Mississippi State Conference on Differential Equations and Computational Simulations, EJDE **10** (2003).

cdn [4] Costa, D., Z. Ding and J. M. Neuberger, *A Numerical Investigation of Sign-Changing Solutions to Superlinear Elliptic Equations on Symmetric Domains*, J. Comput. Appl. Math. **131** (2001), no. 1-2, p299-319.

cm [5] Choi and McKenna, *A Mountain Pass Algorithm ...*

GAP [6] The GAP Group, *GAP – Groups, Algorithms, and Programming,* ; 2002, `http://www.gap-system.org`.

vol2 [7] Golutbitsky, M., I. Stewart and D. G. Schaefer, *Sinularities and groups in bifurcation theory, Volume 2.* Applied Mathematical Sciences **69** Springer-Verlag, New York (1988).

tsp [8] Golutbitsky, M. and I. Stewart *The symmetry perspective: from equilibrium to chaos in phase space and physical space*, Progress in Mathematics **200**, Birkhäuser Verlag, Basel (2002).

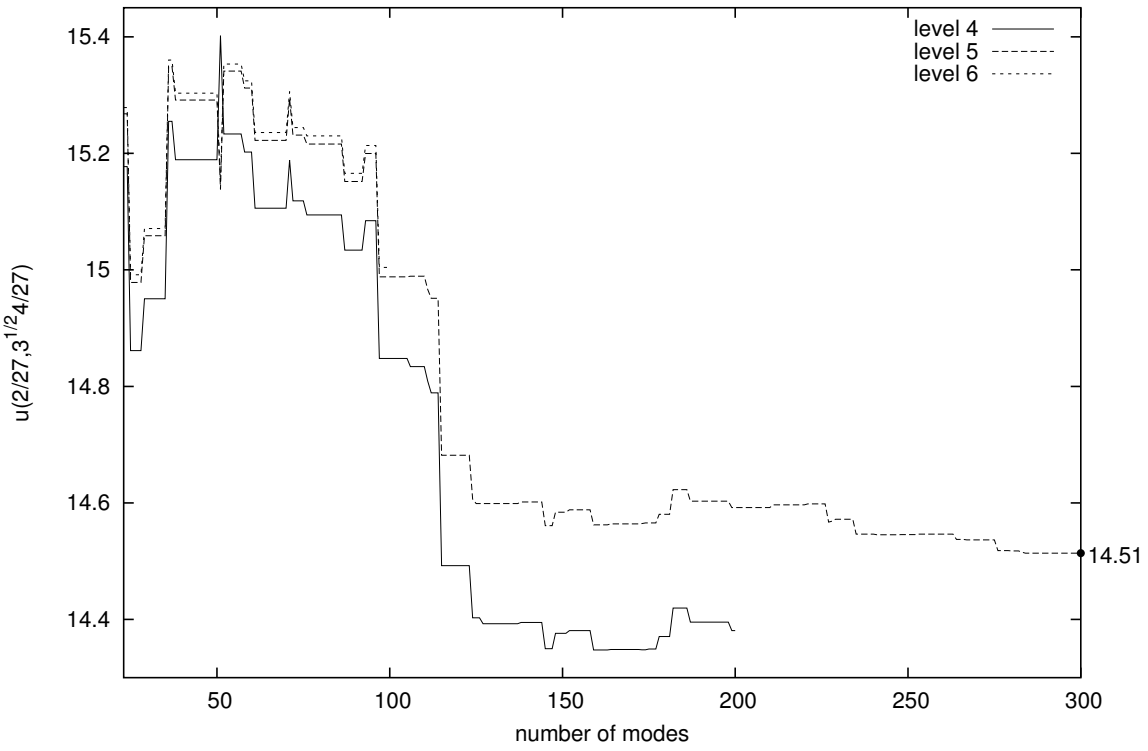

FIGURE 15. A plot of $u(2/27, \sqrt{3}4/27)$ as a function of the number of modes for the solution u at $\lambda = 0$ with symmetry type S_{10}. See Figures 7, 13, and 14 for the location of this solution on bifurcation diagrams. Note that the point labelled with 14.51 matches the point labelled with S_{10} in Figure 7. levelmode

lnrg [9] Lapidus, M. L., J. W. Neuberger, R. L. Renka, and C. A. Griffith, *Snowflake Harmonics and Computer Graphics: Numerical Computation of Spectra on Fractal Drums*, International Journal Bifurcation and Chaos **6** no. 7 (1996), pp 1185–1210.

michel [10] Michel, L. *Nonlinear group action: Smooth actions of compact Lie groups on manifolds* In: Statistical Mechanics and Field Theory (R. N. Sen and C. Weil, Eds.) Israel University Press, Jerusalem, pp. 133-150, (1972).

conm [11] Neuberger, J. M., *GNGA: Recent Progress and Open Problems for Semilinear Elliptic PDE*, to appear in the proceedings of "Variational Methods: Open Problems, Recent Progress, and Numerical Algorithms" conference, Flagstaff, AZ, 2002, AMS J. of Contemp. Math. (2004).

hn [12] Hineman, J. and J. M. Neuberger, *Numerical Solutions to Semilinear Elliptic BVP on Bunimovich Stadia*, Work in Progress.

Jr [13] Johnson, L. and R. Riess, *Numerical Analysis*, Addison-Wesley : Reading, Mass. (1982).

arpack [14] Lehoucq, R. B., D. C. Sorensen, and C. Yang *ARPACK users' guide: Solution of large-scale eigenvalue problems with implicitly restarted Arnoldi methods. Software, Environments, and Tools.* Society for Industrial and Applied Mathematics (SIAM) : Philadelphia, PA. (1998).

matthews [15] Matthews, P. C., *Automated Symmetry-Breaking Calculations*, LMS J. Computational Math. 7 (2004), pp 101–119.

mpa

S	group	possible modes	MPA/MI	MMPA/MI
1	$D_6 \times Z_2$	none	NA	NA
2	$\langle \rho, \sigma \rangle$	1,6,..	S_2/**MI 1**	S_2/**MI 8**
3	$\langle \rho, -\sigma \rangle$	24,37,..	S_3/MI 17	S_3/**MI 17**
4	$\langle -\rho, \sigma \rangle$	7,14,..	S_4/MI 7	S_4/**MI 7**
5	$\langle -\rho, -\sigma \rangle$	10,25,..	S_5/MI 10	S_5/**MI 10**
6	$\langle \sigma, \tau \rangle$	1,6,..,4,11,..	S_2/MI 1	S_6/**MI 4**
7	$\langle -\sigma, -\tau \rangle$	24,37,..,5,12,..	S_7/MI 5	S_7/**MI 5**
8	$\langle \sigma, -\tau \rangle$	7,14,..,2,8,..	S_8/MI 2	S_8/**MI 2**
9	$\langle -\sigma, \tau \rangle$	10,25,..3,9,..	S_9/MI 3	S_9/**MI 3**
10	$\langle \rho \rangle$	1,6,..,24,37,..	S_2/MI 1	S_2/MI 8
11	$\langle \rho^2, \sigma \rangle$	1,6,..,7,14,..	S_2/MI 1	S_{11}/**MI 6**
12	$\langle \rho^2, \tau \rangle$	1,6,..,10,25,..	S_2/MI 1	S_{12}/**MI 7**
13	$\langle \rho^2, -\tau \rangle$	7,14,..,24,37,..	S_4/MI 7	S_4/MI 7
14	$\langle \rho^2, -\sigma \rangle$	10,25,..,24,37,..	S_5/MI 10	S_5/MI 10
15	$\langle -\rho \rangle$	7,14,..,10,25,..	S_4/MI 7	S_4/MI 7
16	$\langle \rho^2 \rangle$	1,6,..,24,37,..,7,14,.,.10,25,..	S_2/MI 1	S_{11}/MI 6
17	$\langle \rho^3 \rangle$	1,6,..,24,37,..,4,11,..,5,12,..	S_2/MI 1	S_{17}/**MI 4**
18	$\langle \sigma \rangle$	1,6,..,7,14,..,..,4,11,..,2,8,..	S_2/MI 1	S_8/MI 2
19	$\langle \tau \rangle$	1,6,..,10,25,..,4,11,..,3,9,..	S_2/MI 1	S_9/MI 3
20	$\langle -\tau \rangle$	24,37,..,7,14,..,5,12,..,2,8,..	S_8/MI 2	S_8/MI 2
21	$\langle -\sigma \rangle$	24,37,..,10,25,..,5,12,..,3,9,..	S_9/MI 3	S_9/MI 3
22	$\langle -\rho^3 \rangle$	7,14,..,10,25,..,2,8,..,3,9..	S_8/MI 2	S_8/MI 2
23	$\langle 1 \rangle$	all	S_2/MI 1	S_8/MI 2

TABLE 5. Symmetries, MPA and MMPA for invariant subspaces, and MI. Bold entries indicate a non-redundant solution. For convenience, the first two possibly nonzero mode numbers for each component of the invariant subspace are provided.

nnn [16] Neuberger, B., J.W. Neuberger, and D.W. Noid *Eigenfunctions on a Stadium Associated With Avoided Crossings of Energy Levels*

num [17] Neuberger, J. M., *Numerical ...*

graph [18] Neuberger, J. M., *Nonlinear Elliptic Partial Difference Equations on Graphs*, preprint, submitted (2003).

ns [19] Neuberger, J. M. and J. W. Swift *Newton's method and Morse index for semilinear elliptic PDEs* International Journal Bifurcation and Chaos **11** no. 3 (2001), pp 801–820.

nss [20] Neuberger, J. M., N. Sieben and J. W. Swift, *Computing Eigenfunctions on the Koch Snowflake: A New Grid and Symmetry*, submitted for publication (2004).

rab [21] Rabinowitz, P., *Minimax Methods in Critical Point Theory with Applications to Differential Equations*, Regional Conference Series in Mathematics, **65**, AMS : Providence, R.I. (1986).

sagan [22] Sagan, B. E. *The symmetric group*, Wadsworth & Brooks/Cole Adv. Books Software, Pacific Grove, CA, 1991.

scott [23] Scott, W. R. *Group theory*, Prentice Hall, Englewood Cliffs, N.J., 1964.

smoller [24] Smoller, J. and A. G. Wasserman, *Symmetry-Breaking for Positive Solutions of Semilinear elliptic equations* Archives of Rational Mechanics Analysis **95**, pp. 217-225 (1986).

sternberg [25] Sternberg, S. *Group Theory and Physics* Cambridge University Press, Cambridge (1994).

tinkam [26] Tinkham, M. *Group Theory and Quantum Mechanics* McGraw-Hill Inc., New York (1964).

E-mail address: John.Neuberger@nau.edu, Nandor.Sieben@nau.edu, Jim.Swift@nau.edu

Department of Mathematics and Statistics, Northern Arizona University PO Box 5717, Flagstaff, AZ 86011-5717, USA